

Tensor Method for Optimal Control Problems Constrained by Fractional 3D Elliptic Operator with Variable Coefficients

Britta Schmitt* Boris N. Khoromskij† Venera Khoromskaia‡
Volker Schulz§

Abstract

We introduce the tensor numerical method for solving optimal control problems that are constrained by fractional 2D and 3D elliptic operators with variable coefficients. We solve the governing equation for the control function which includes a sum of the fractional operator and its inverse, both discretized over large 3D $n \times n \times n$ spacial grids. Using the diagonalization of the arising matrix valued functions in the eigenbasis of the 1D Sturm-Liouville operators, we construct the rank-structured tensor approximation with controllable precision for the discretized fractional elliptic operators and the respective preconditioner. The right-hand side in the constraining equation (the optimal design function) is supposed to be represented in a form of a low-rank canonical tensor. Then the equation for the control function is solved in a tensor structured format by using preconditioned CG iteration with the adaptive rank truncation procedure that also ensures the accuracy of calculations, given an ε -threshold. This method reduces the numerical cost for solving the control problem to $O(n \log n)$ (plus the quadratic term $O(n^2)$ with a small weight), which is superior to the approaches based on the traditional linear algebra tools that yield at least $O(n^3 \log n)$ complexity in the 3D case. The storage for the representation of all 3D nonlocal operators and functions involved is also estimated by $O(n \log n)$. This essentially outperforms the traditional methods operating with fully populated $n^3 \times n^3$ matrices and vectors in \mathbb{R}^{n^3} . Numerical tests for 2D/3D control problems indicate the almost linear complexity scaling of the rank truncated PCG iteration in the univariate grid size n .

Key words: Fractional elliptic operators, low-rank tensor approximations, optimal control problems, Tucker and canonical tensor formats.

AMS Subject Classification: 65F30, 65F50, 65N35, 65F10

*University of Trier, FB 4 - Department of Mathematics, D-54296, Trier, Germany (schmittb@uni-trier.de).

†Max-Planck-Institute for Mathematics in the Sciences, Inselstr. 22-26, D-04103 Leipzig, Germany (bokh@mis.mpg.de); University of Trier, FB 4 - Department of Mathematics, D-54296, Trier.

‡Max Planck Institute for Mathematics in the Sciences, Leipzig, Germany (vekh@mis.mpg.de).

§University of Trier, FB 4 - Department of Mathematics, D-54296, Trier, Germany (volker.schulz@uni-trier.de).

1 Introduction

Optimization problems that are constrained by partial differential equations (PDEs) have a long history in mathematical literature since they allow a huge number of applications in different fields of natural science, see [43, 1, 25] for some comprehensive examples. Being studied for many years, tracking-type problems which trace the discrepancy between the solution of the PDE and a given target state represent a very important class of optimal control problems [13]. In such problems the discretization and numerical treatments of the elliptic PDE in constraints that determines the relation between the optimal design and control functions,

$$\mathcal{L}y = u,$$

can be performed by the traditional FEM methods dealing with sparse matrices. Multigrid methods for elliptic equations are shown to be efficient since their computational complexity is linear in the number of grid points in the computational domain in \mathbb{R}^d , see [8, 9].

The construction of suitable discretization and solution schemes become a challenging task whenever the operator \mathcal{L} in the constraint equation inherits nonlocal structures, such as for instance in the case of a fractional differential operator, that is \mathcal{L}^α . In recent years, considering fractional PDEs is gaining more attention due to an higher accuracy within the numerical simulation of the real world problems, for example in the subject areas concerning heat diffusion in special materials [7], image processing [19], material science [5], optimization [17]. For more application areas see [2] and references therein.

However, as the pay-off for higher modeling accuracy in applications, fractional operators in PDEs also imply nonlocality to the given equation, which after discretization leads to dense problem structures resulting in quadratic complexity in the number of degrees of freedom in \mathbb{R}^d , so that they are hard to handle especially when large grids are considered in many dimensions. As a result, common numerical solution approaches lead to severe problems, such that a number of special techniques has been advocated [26, 45, 16, 27, 4].

Furthermore, the possible presence of variable coefficients within the PDE has a huge impact on the numerical complexity of a suitable solution technique. In this case, assuming separability for the involved coefficients in \mathbb{R}^d leads to favorable, highly structured matrices after discretization that allow using efficient numerical representations such as Kronecker product structures [33, 38, 39, 14] and the respective multilinear algebra.

In this article, we consider a tracking-type optimal control problem constrained by a fractional Laplace type elliptic operator with variable, separable coefficients discretized on a tensor grid. For an overview about several characterizations of the fractional elliptic operators and the respective algebra see [18, 28, 26, 40, 41]. A number of application fields motivating the use of fractional power of elliptic operators, for example in biophysics, mechanics, nonlocal electrostatics and image processing have been discussed in the literature [3, 2, 15, 45, 16, 27, 30]. In such applications control problems arise naturally.

An application of standard numerical methods for the solution of PDEs in \mathbb{R}^d is essentially limited by the so-called *curse of dimensionality* [6], that is the effect of an exponential growth of storage and computational complexity, $O(n^d)$, in the dimension of the problem d , where n is the univariate grid size of the discretization. This phenomenon effects all basic procedures such as matrix-vector calculus and full format matrix arithmetics. Some special numerical

techniques like adaptive h-p mesh refinement, sparse grids [10], hierarchical matrices [22] and fast multipole methods [20] only partially relax the curse of dimensionality.

The modern tensor numerical methods, based on low-rank separable approximation of operators and functions in \mathbb{R}^d , are capable to reduce the numerical cost in higher dimensions to the linear scaling in d , $O(dn)$, thus making possible the efficient numerical modeling in higher dimensions. Meanwhile, tensor decompositions using canonical and Tucker tensor formats and the respective multilinear algebra techniques have been used since long in the computer science for data analysis and signal processing [44, 12, 11, 37]. The Tucker approximation tools are based on the principal generalization of the singular value decomposition (SVD) called the higher order SVD (HOSVD) [12]. However, the analytical methods of separable low-rank representation of multivariate functions and operators [42, 23, 18, 32] appeared to be the main prerequisite to tensor numerical calculus. Tensor numerical methods in scientific computing have been first introduced for calculation of the 3D convolution integral operators with Green's kernels in quantum chemistry, see [31] for the detailed discussion.

In the recent decade tensor formats created specifically for the solution of multidimensional problems have been introduced in the form of tensor train and quantized tensor train representations, hierarchical tensors, and the recent range-separated tensor decomposition. Finally, the main feature of the tensor numerical techniques in scientific computing is the arrangement and usage of separable data structures in order to reduce the solution of given multidimensional equations to essentially one-dimensional operations, see [21, 34, 31] for the detailed discussion and comprehensive references.

In the present paper, we proceed with the development of efficient tensor numerical techniques for the solution of optimal control problems which were initiated in [24] for solving control problem with 2D and 3D classical fractional Laplace operator in constraints. In the latter case one could use the FFT-based diagonalization of the fractional Laplacian to construct the rank-structured representation of the governing nonlocal operator. In our problem setting we essentially generalize the previous approach to a more general class of tracking-type optimal control problems in \mathbb{R}^d , $d = 2, 3$, constrained by a PDE containing a fractional divergence type elliptic operator with variable coefficients.

Since the FFT-based factorizations may no longer be applied, we use the diagonalization of the arising fully populated matrix valued functions in the eigen-basis of the 1D Sturm-Liouville operators. The diagonal of the coefficients matrix in the factorized representation of the resulting governing operator (in the product of 1D eigen-bases) is reshaped to a third-order tensor which undergoes the rank-structured decomposition by using the multigrid Tucker-to-canonical tensor transform [36]. The spectrally equivalent preconditioner with small Kronecker rank (K -rank) is constructed by using the decomposition of the fractional anisotropic Laplace operator in the Fourier basis, and by subsequent low-rank approximation via the multigrid Tucker algorithm. Then the discrete linear system is solved by the preconditioned conjugate gradient (PCG) iteration with adaptive rank truncation adapting the rank-structured tensor representation of all involved quantities: the governing operator, the preconditioner, the right hand side as well the solution vector. The adaptive rank reduction for the solution vector in the course of PCG iteration is performed by using the canonical-to-Tucker decomposition via the reduced HOSVD (RHOSVD), see [36, 31]. The numerical accuracy is controlled by the given ε -threshold in the rank reduction procedure of the algorithm RHOSVD.

Finally, we apply the above methods to solve a tracking-type optimal control problem constrained by a PDE with a fractional divergence type elliptic operator with variable coefficients discretized on $n \times n \times n$ Cartesian grid in \mathbb{R}^3 . Our approach exhibits the linear complexity scaling in dimension, $O(dn^2)$. The theoretical justification for the use of aforementioned tensor approximations can be found in [23, 18, 34], see also [24] where the classical fractional Laplace operator $(-\Delta)^\alpha$ in constraints was discussed and analyzed.

The rest of the paper is structured as follows. Section 2 describes the target class of optimal control problems and the special definitions that come with a separable structure of the involved fractional elliptic operator. In section 3 the discrete optimality equation system is derived with the help of the Lagrangian multiplier approach. Afterwards, the discretization of the control problem is developed and the Laplace-type operator with variable coefficients is decomposed with the help of factorized low-rank structures. We also recapitulate the low-rank structures used for the preconditioner. The presented techniques are then used in a special tailored PCG algorithm with adaptive rank truncation. Finally, in section 4 we present and analyze our numerical results for 2D and 3D examples and discuss aspects related to computation and storage complexities when solving the considered class of optimal control problems by using tensor numerical method combined with the introduced PCG iterative algorithm.

2 Problem setting

Our goal is the construction of fast tensor numerical solution schemes for solving the control problems constrained by fractional d -dimensional elliptic operators with variable coefficients. For this reason we restrict ourself to the case of rectangular domains and to the class of elliptic operators with diagonal separable coefficients.

Given the design function $y_\Omega \in L^2(\Omega)$ on $\Omega := (0, 1)^d$, $d = 1, 2, 3$, first, we consider the optimization problem for the cost functional

$$\min_{y,u} J(y, u) := \int_{\Omega} (y(x) - y_\Omega(x))^2 dx + \frac{\gamma}{2} \int_{\Omega} u^2(x) dx, \quad (2.1)$$

constrained by the elliptic boundary value problem in Ω for the state variable $y \in H_0^1(\Omega)$,

$$\mathcal{A}y := -\nabla^T \cdot \mathbb{A}(x)\nabla y = \beta u, \quad x \in \Omega, \quad u \in L_2(\Omega), \quad \beta > 0, \quad (2.2)$$

endorsed with the homogeneous Dirichlet (or periodic) boundary conditions on $\Gamma = \partial\Omega$, i.e., $y|_\Gamma = 0$. The coefficient matrix $\mathbb{A}(x) \in \mathbb{R}^{d \times d}$ is supposed to be symmetric, positive definite and uniformly bounded in Ω with positive constants $c > 0$ and $C > 0$, i.e.,

$$c I_{d \times d} \leq \mathbb{A}(x) \leq C I_{d \times d}.$$

Under above assumptions the associated bilinear form

$$A(u, v) = \int_{\Omega} \mathbb{A}(x)\nabla u(x) \cdot \nabla v(x) dx$$

defined on $V \times V$, $V := \{v \in H_0^1(\Omega)\}$ is symmetric, coercive and bounded on V with the same constants c and C .

In what follows, we consider for $0 < \alpha \leq 1$ the control problems constrained by the fractional elliptic operator

$$\mathcal{A}^\alpha y = \beta u, \quad u \in L_2(\Omega), \quad \beta > 0 \quad (2.3)$$

with the spectral definition of the fractional power of the elliptic operator \mathcal{A} by

$$\mathcal{A}^\alpha y(x) = \sum_{i=1}^{\infty} \lambda_i^\alpha c_i \psi_i(x), \quad y = \sum_{i=1}^{\infty} c_i \psi_i(x),$$

where $\{\psi_i(x)\}_{i=1}^{\infty}$ is the set of L_2 -orthogonal eigenfunctions of the symmetric, positive definite operator \mathcal{A} , while $\{\lambda_i\}_{i=1}^{\infty}$ are the corresponding (real and positive) eigenvalues.

The numerical efficiency of this approach is based on the exponentially fast convergence of the sinc quadratures on a class of analytic functions. This technique is to be applied in the present paper for the theoretical analysis of the rank decomposition schemes, for the description of their constructive representation and for the design of spectrally close preconditioners for the governing equations based on the use of fractional Laplacian.

The linear constraint equation (2.3) allows to eliminate the state variable and then to derive the Lagrange equation for the control u in the explicit form as follows (see §3 concerning the Lagrange equations)

$$\mathcal{F}(\mathcal{A})u := (\beta \mathcal{A}^{-\alpha} + \frac{\gamma}{\beta} \mathcal{A}^\alpha)u = y_\Omega, \quad (2.4)$$

for some positive constants $\beta > 0$ and $\gamma > 0$. The equation for the state variable reads

$$y = \beta \mathcal{A}^{-\alpha} u. \quad (2.5)$$

The practically interesting range of parameters includes the case $\beta = O(1)$ for small values of $\gamma > 0$.

The presented numerical scheme is focused on the solution of discrete versions of equations (2.4) and (2.5) that include a nonlocal elliptic operator \mathcal{A}^α and its inverse $\mathcal{A}^{-\alpha}$. The efficiency of the rank-structured tensor approximations presupposes that the design function on the right-hand side of these equations, $y_\Omega(x_1, x_2, x_3)$, allows the low-rank separable approximation.

Since we aim for the low-rank (approximate) tensor representation of all functions and operators involved in the above formulation of the control problem, we further assume that the equation coefficients matrix takes a diagonal form

$$\mathbb{A}(x) = \text{diag}\{a_1(x_1), a_2(x_2)\}, \quad a_\ell(x_\ell) > 0, \quad \ell = 1, 2, \quad (2.6)$$

in 2D case and similar for $d = 3$,

$$\mathbb{A}(x) = \text{diag}\{a_1(x_1), a_2(x_2), a_3(x_3)\}, \quad a_\ell(x_\ell) > 0, \quad \ell = 1, 2, 3. \quad (2.7)$$

Hence, we consider the optimal control problem constrained by fractional elliptic operator with separable coefficients, such that the equation (2.3) takes form

$$\mathcal{A}^\alpha y = \left(- \sum_{\ell=1}^d \frac{\partial}{\partial x_\ell} a_\ell(x_\ell) \frac{\partial}{\partial x_\ell} \right)^\alpha y = \beta u, \quad 0 \leq \alpha \leq 1. \quad (2.8)$$

Notice that the efficient tensor numerical method for the case of fractional Laplace operator in constraint, i.e., $a_\ell(x_\ell) = 1$, $\ell = 1, 2, 3$, was developed in [24].

For a rank structured representation of the elliptic operator inverse (and some other operator valued functions $f(\mathcal{A})$) one can apply the integral representation based on the Laplace type transform [26],

$$\mathcal{A}^{-\alpha} = \frac{1}{\Gamma(\alpha)} \int_0^\infty t^{\alpha-1} e^{-t\mathcal{A}} dt, \quad (2.9)$$

which suggests the numerical schemes for low-rank canonical tensor representation of the operator (matrix) $\mathcal{A}^{-\alpha}$ by using the sinc quadrature approximations for the integral on the real axis [18],

$$\int_0^\infty t^{\alpha-1} e^{-t\mathcal{A}} dt \approx \sum_{k=-M}^M \hat{c}_k t_k^{\alpha-1} e^{-t_k \mathcal{A}} = \sum_{k=-M}^M c_k \bigotimes_{\ell=1}^d e^{-t_k A_\ell}, \quad (2.10)$$

applied to the operators composed by a sum of commutable terms,

$$\mathcal{A} = \sum_{\ell=1}^d A_\ell, \quad [A_\ell, A_k] = 0, \quad \text{for all } \ell, k = 1, \dots, d, \quad (2.11)$$

which ensures that each summand in (2.10) is separable, i.e. $e^{-t_k \mathcal{A}} = \bigotimes_{\ell=1}^d e^{-t_k A_\ell}$. For example, in the case of the target class of operators in (2.8), (2.11), we obtain the d -term decomposition

$$\mathcal{A} = - \sum_{\ell=1}^d \frac{\partial}{\partial x_\ell} a_\ell(x_\ell) \frac{\partial}{\partial x_\ell}$$

with *commutable* 1D operators $A_\ell = -\frac{\partial}{\partial x_\ell} a_\ell(x_\ell) \frac{\partial}{\partial x_\ell}$, for $\ell = 1, \dots, d$.

In this paper we consider the discrete matrix formulation of the optimal control problem (2.1) constrained by (2.2) based on a FEM/FDM discretization A_h of a d -dimensional elliptic operator \mathcal{A} defined on the uniform $n_1 \times n_2 \times \dots \times n_d$ tensor grid in Ω , where $h = h_\ell = 1/n_\ell$ is the univariate mesh parameter. The L_2 scalar product is substituted by the Euclidean scalar product (\cdot, \cdot) of multi-indexed vectors in $\mathbb{R}^{\mathbf{n}}$, $\mathbf{n} = (n_1, n_2, \dots, n_d)$.

The fractional elliptic operators $\mathcal{A}^{\pm\alpha}$ are approximated by their FEM/FDM representation $(A_h)^{\pm\alpha}$, where the matrix $(A_h)^{\pm\alpha}$ is defined in terms of spectral decomposition of A_h .

3 Rank-structured representation of operator valued functions of interest

The numerical treatment of minimization problem (2.1) with constraint (2.3) requires solving the corresponding Lagrange equation for the necessary optimality conditions. In this section, we will derive these conditions based on a discretize-then-optimize-approach. Afterwards, we will discuss how the involved discretized operators can be applied efficiently in a low-rank format, and how this can be used to design a preconditioned conjugate gradient (PCG) scheme for the necessary optimality conditions.

3.1 Discrete optimality conditions

We present the necessary first order conditions based on their derivation in [24].

We consider a version of the control problem (2.1) constrained by (2.3), discretized on a uniform grid in each dimension,

$$\begin{aligned} \min_{\mathbf{y}, \mathbf{u}} &= \frac{1}{2}(\mathbf{y} - \mathbf{y}_\Omega)^T M(\mathbf{y} - \mathbf{y}_\Omega) + \frac{\gamma}{2} \mathbf{u}^T M \mathbf{u} \\ \text{s. t. } & A^\alpha \mathbf{y} = \beta M \mathbf{u}, \end{aligned}$$

where vectors $\mathbf{y}, \mathbf{y}_\Omega, \mathbf{u} \in \mathbb{R}^N$ denote the discretized state y , design y_Ω and control u , respectively. The discretization of the elliptic operator \mathcal{A} by finite elements or finite differences is denoted by $A = A_h$. The matrix M will be a mass matrix in the finite element case and simply the identity matrix in the finite difference case.

Setting up the Lagrangian function with the help of the discrete adjoint variable \mathbf{p} ,

$$L(\mathbf{y}, \mathbf{u}, \mathbf{p}) = \frac{1}{2}(\mathbf{y} - \mathbf{y}_\Omega)^T M(\mathbf{y} - \mathbf{y}_\Omega) + \frac{\gamma}{2} \mathbf{u}^T M \mathbf{u} + \mathbf{p}^T (A^\alpha \mathbf{y} - \beta M \mathbf{u}),$$

and deriving it with respect to all three variables, we end up with the equation system

$$\begin{bmatrix} M & O & A^\alpha \\ O & \gamma M & -\beta M \\ A^\alpha & -\beta M & O \end{bmatrix} \begin{pmatrix} \mathbf{y} \\ \mathbf{u} \\ \mathbf{p} \end{pmatrix} = \begin{pmatrix} \mathbf{y}_\Omega \\ \mathbf{0} \\ \mathbf{0} \end{pmatrix} \begin{matrix} \text{(I)} \\ \text{(II)} \\ \text{(III)} \end{matrix}.$$

The system contains the necessary first order optimality conditions belonging to the discussed optimal control problem.

Then the state equation (III) can be solved for \mathbf{y} , yielding

$$\mathbf{y} = \beta A^{-\alpha} \mathbf{u}. \quad (3.1)$$

Subsequently to solving (II) for \mathbf{p} , the adjoint equation (I) eventually provides an equation for the control \mathbf{u} , that is

$$(\beta A^{-\alpha} + \frac{\gamma}{\beta} A^\alpha) \mathbf{u} = \mathbf{y}_\Omega. \quad (3.2)$$

In what follows, we describe how to derive the discretization of the operator \mathcal{A} and afterwards present the efficient tensor based numerical method for solving equation (3.2) and related ones.

3.2 Finite difference scheme

First, we derive a factorized representation of the discrete elliptic operator A and the related matrix valued functions of A , which are compatible with low-rank data. Let $I_{(\ell)}$ denote the identity matrix, and $A_{(\ell)}$ the discretized one-dimensional Sturm-Liouville operators on the given grid in the ℓ th mode, then we have

$$A \equiv A_1 \oplus A_2 \oplus A_3 = A_{(1)} \otimes I_2 \otimes I_3 + I_1 \otimes A_{(2)} \otimes I_3 + I_1 \otimes I_2 \otimes A_{(3)}, \quad (3.3)$$

where \otimes denotes the Kronecker product of matrices.

To obtain the symmetric three-diagonal matrices $A_{(\ell)}$, $\ell = 1, 2, 3$, we simply discretize the one-dimensional Sturm-Liouville eigenvalue problems

$$\begin{aligned} -\frac{\partial}{dx_\ell} a_\ell(x_\ell) \frac{\partial}{dx_\ell} y &= \lambda y, \\ y(0) &= y(1) = 0. \end{aligned} \quad (3.4)$$

Therefore, we use the corresponding weak formulation

$$\int_0^1 -a_\ell(x_\ell) p'(x_\ell) y'(x_\ell) dx_\ell = \int_0^1 -\lambda y(x_\ell) p(x_\ell) dx_\ell \quad (3.5)$$

for $\Omega =]0, 1[$ and $p(x_\ell) \in C^1(]0, 1[) \cap C([0, 1])$, $p(0) = 0 = p(1)$, $\ell = 1, 2$.

For the sake of simplicity we set $a := a_\ell$ and consider a uniform grid with grid size $h := h_\ell$.

For discretization, we use the finite difference approximations

$$p'_i = \frac{p_i - p_{i-1}}{h} \quad \text{and} \quad y'_i = \frac{y_i - y_{i-1}}{h}$$

as well as the evaluation $a_{i \pm \frac{1}{2}}$ of the equation coefficients $a_\ell(x_\ell)$ at the middle point of two grid points.

Finally, we end up with the following discretization for above weak formulation (3.5). Considering the left side of (3.5), the discretization reads

$$\begin{aligned} & \int_0^1 -a_\ell(x_\ell) p'(x_\ell) y'(x_\ell) dx_\ell \\ = & -h \sum_{i=2}^{n(\ell)} a_{i-\frac{1}{2}} \frac{p_i - p_{i-1}}{h} \frac{y_i - y_{i-1}}{h} \\ = & -h \sum_{i=2}^{n(\ell)} a_{i-\frac{1}{2}} \frac{y_i - y_{i-1}}{h^2} (p_i - p_{i-1}) \\ = & -h \sum_{i=2}^{n(\ell)} a_{i-\frac{1}{2}} \frac{y_i - y_{i-1}}{h^2} p_i + h \sum_{i=1}^{n(\ell)-1} a_{i+\frac{1}{2}} \frac{y_{i+1} - y_i}{h^2} p_i \\ = & h a_{1+\frac{1}{2}} \frac{y_2 - y_1}{h^2} p_1 - h \sum_{i=2}^{n(\ell)-1} \left(a_{i-\frac{1}{2}} \frac{y_i - y_{i-1}}{h^2} - a_{i+\frac{1}{2}} \frac{y_{i+1} - y_i}{h^2} \right) p_i - h a_{n(\ell)-\frac{1}{2}} \frac{y_{n(\ell)} - y_{n(\ell)-1}}{h^2} p_{n(\ell)}, \end{aligned}$$

whereas for the right side of (3.5), it holds that

$$\int_0^1 -\lambda y(x_\ell) p(x_\ell) dx_\ell = -\lambda h \sum_{i=2}^{n(\ell)-1} y_i p_i - h \frac{y_1 p_1}{2} - h \frac{y_{n(\ell)} p_{n(\ell)}}{2}.$$

Ultimately, the full discretization scheme for the one-dimensional eigenvalue problem (3.4) is

$$\underbrace{-\frac{1}{h_\ell^2} \begin{bmatrix} a_{1,1} & a_{1,2} & & & \\ a_{2,1} & a_{2,2} & a_{2,3} & & \\ & \ddots & \ddots & & \\ & & a_{n_\ell, n_\ell-1} & a_{n_\ell, n_\ell} & \\ & & & & \end{bmatrix}}_{=A_\ell} \begin{pmatrix} y_1 \\ \vdots \\ y_{n_\ell} \end{pmatrix} = \lambda \begin{pmatrix} y_1 \\ \vdots \\ y_{n_\ell} \end{pmatrix}.$$

with the entries of the three-diagonal matrix $A = [a_{i,j}]$ given by (we skip the subindex ℓ)

$$a_{i,j} = \begin{cases} a_{i+\frac{1}{2}} & j - i = 1 \\ a_{i-\frac{1}{2}} & j - i = -1 \\ -a_{i+\frac{1}{2}} - a_{i-\frac{1}{2}} & i = j, \quad i \notin \{1, n(\ell)\} \\ -2a_{i+\frac{1}{2}} & i = j = 1 \\ -2a_{i-\frac{1}{2}} & i = j = n(\ell). \end{cases}$$

3.3 Stiffness matrix in the low-rank Kronecker form

Again, consider the Laplace-type operator A in discretized format (3.3), that is

$$A = A_{(1)} \otimes I_2 \otimes I_3 + I_1 \otimes A_{(2)} \otimes I_3 + I_1 \otimes I_2 \otimes A_{(3)}.$$

Let $G_\ell \in \mathbb{R}^{n_\ell \times n_\ell}$ be the orthogonal matrix composed of the eigenvectors of the problem

$$A_{(\ell)} g_i = \lambda_i^{(\ell)} g_i, \quad g_i \in \mathbb{R}^{n_\ell}, \quad i \in \{1, \dots, n_\ell\}. \quad (3.6)$$

Then the one-dimensional operator (matrix) $A_{(\ell)}$ admits an eigenvalue decomposition in its eigenbasis,

$$A_{(\ell)} = G_\ell^T A_{(\ell)} G_\ell, \quad A_{(\ell)} = \text{diag}\{\lambda_1^{(\ell)}, \dots, \lambda_{n_\ell}^{(\ell)}\}, \quad \ell = 1, 2, 3$$

with G_ℓ consisting of the (column) eigenvectors $g_i \in \mathbb{R}^{n_\ell}$.

Following [24] and using the properties of the Kronecker product, we can write the first summand in (3.3) as

$$\begin{aligned} A_{(1)} \otimes I_2 \otimes I_3 &= (G_1^T A_{(1)} G_1) \otimes (G_2^T I_2 G_2) \otimes (G_3^T I_3 G_3) \\ &= (G_1^T \otimes G_2^T \otimes G_3^T) (A_{(1)} \otimes I_2 \otimes I_3) (G_1 \otimes G_2 \otimes G_3), \end{aligned}$$

and similarly for matrices $A_{(2)}$ and $A_{(3)}$. Eventually, this suggests the following rank-3 Kronecker representation of the full stiffness matrix in (3.3) as

$$A = (G_1^T \otimes G_2^T \otimes G_3^T) [A_1 \otimes I_2 \otimes I_3 + I_1 \otimes A_2 \otimes I_3 + I_1 \otimes I_2 \otimes A_3] (G_1 \otimes G_2 \otimes G_3). \quad (3.7)$$

Considering $d = 2$, expression (3.7) simplifies to

$$\begin{aligned} A &= (G_1^T \otimes G_2^T) (A_1 \otimes I_2) (G_1 \otimes G_2) + (G_1^T \otimes G_2^T) (I_1 \otimes A_2) (G_1 \otimes G_2) \\ &= (G_1^T \otimes G_2^T) \underbrace{(A_1 \otimes I_2 + I_1 \otimes A_2)}_{=: A} (G_1 \otimes G_2), \end{aligned}$$

which provides the eigenvalue decomposition for any matrix valued function $\mathcal{F}(A)$,

$$\mathcal{F}(A) = (G_1^T \otimes G_2^T) \mathcal{F}(A) (G_1 \otimes G_2). \quad (3.8)$$

Then the eigenvalue decompositions (3.7) and (3.8) provide the efficiently computation of some matrix valued functions $\mathcal{F}(A)$ at the low cost of the order of $O(dn^2)$.

Again following [24], let us assume that $\mathcal{F}(A)$ can be expressed approximately by a linear combination of Kronecker rank-1 operators, so that due to (3.8), for the approximation of $\mathcal{F}(A)$ it is sufficient to approximate the diagonal matrix $\mathcal{F}(\Lambda)$. Thus, we assume the decomposition

$$\mathcal{F}(\Lambda) \approx \sum_{k=1}^R \text{diag}(\mathbf{u}_1^{(k)} \otimes \mathbf{u}_2^{(k)}), \quad (3.9)$$

with vectors $\mathbf{u}_{(\ell)}^{(k)} \in \mathbb{R}^{n_{(\ell)}}$ and $R \ll \min(n_1, n_2)$, and let $\mathbf{x} \in \mathbb{R}^N$ be a vector given in a low-rank format, i. e.

$$\mathbf{x} \approx \sum_{j=1}^S \mathbf{x}_1^{(j)} \otimes \mathbf{x}_2^{(j)},$$

with vectors $\mathbf{x}_{(\ell)}^{(j)} \in \mathbb{R}^{n_{(\ell)}}$ and $S \ll \min(n_1, n_2)$.

Then, we can compute a matrix-vector product

$$\begin{aligned} \mathcal{F}(A)\mathbf{x} &\approx (G_1^T \otimes G_2^T) \left(\sum_{k=1}^R \text{diag}(\mathbf{u}_1^{(k)} \otimes \mathbf{u}_2^{(k)}) \right) (G_1 \otimes G_2) \left(\sum_{j=1}^S \mathbf{x}_1^{(j)} \otimes \mathbf{x}_2^{(j)} \right) \\ &= \sum_{k=1}^R \sum_{j=1}^S G_1^T(\mathbf{u}_1^{(k)} \odot G_1 \mathbf{x}_1^{(j)}) \otimes G_2^T(\mathbf{u}_2^{(k)} \odot G_2 \mathbf{x}_2^{(j)}), \end{aligned} \quad (3.10)$$

where \odot denotes the componentwise (Hadamard) product of vectors.

Expression (3.10) can be calculated in factored form in $\mathcal{O}(RSn^2)$ flops, where $n = \max(n_1, n_2)$.

Considering $d = 3$, with completely analogous reasoning, equation (3.10) becomes

$$\mathcal{F}(A)\mathbf{x} \approx \sum_{k=1}^R \sum_{j=1}^S G_1^T(\mathbf{u}_1^{(k)} \odot G_1 \mathbf{x}_1^{(j)}) \otimes G_2^T(\mathbf{u}_2^{(k)} \odot G_2 \mathbf{x}_2^{(j)}) \otimes G_3^T(\mathbf{u}_3^{(k)} \odot G_3 \mathbf{x}_3^{(j)}), \quad (3.11)$$

which can be implemented with the same asymptotic cost as in 2D case, i.e., in $\mathcal{O}(RSn^2)$ operations.

Remark 3.1 *In the d -dimensional case we arrive at the linear scaling in d of numerical cost, $\mathcal{O}(dRSn^2)$, such that the effect of quadratic scaling in the univariate grid size n becomes negligible in comparison with the gain from getting rid of the curse of dimensionality. Moreover, the cubic cost of solving the eigenvalue problem for $n \times n$ three-diagonal matrix can be considered as negligible in the practically interesting range of grid-size n until several thousand, since it only takes few seconds even for rather large matrices, see also section 4.1 for more details.*

It is worth to note that in the case of non-structured (full format) long vectors $\mathbf{x} \in \mathbb{R}^{n^3}$ we have $S = n^2$ which increases the cost of matrix-vector multiplication up to $\mathcal{O}(Rn^4)$.

In our applications we are interested in the low Kronecker rank (K -rank) representations (approximations) of the matrix valued functions

$$\mathcal{F}_1(A) = A^\alpha, \quad \mathcal{F}_2(A) = A^\alpha + A^{-\alpha}, \quad \text{and} \quad \mathcal{F}_3(A) = (A^\alpha + A^{-\alpha})^{-1},$$

where $A = A_h$ is the FEM/FDM discretization of the target elliptic operator \mathcal{A} . Another important task is the construction of the spectrally close low K -rank preconditioners for the matrix valued function $\mathcal{F}_2(A)$. These issues will be discussed in the next sections.

3.4 Low-rank approximation and the Kronecker rank bounds

First we notice that the orthogonal transformation matrix $G_1 \otimes G_2 \otimes G_3$ in the factorization (3.7) has Kronecker rank 1. This means that the low K -rank decomposition of the matrix valued function $\mathcal{F}(A)$ is equivalent to the low-rank tensor approximation of the 3-way folding of the diagonal matrix $\mathcal{F}(\Lambda)$. If we suppose that the initial system matrix A is spectrally equivalent to the anisotropic Laplacian (see details in §3.5 below) then the existence of the low-rank approximation for the target matrix valued function $\mathcal{F}(A)$, in particular $\mathcal{F}_2(A)$ could be justified by slightly modified argument of those applied in [24] for the case of discrete Laplacian.

In what follows, we discuss the Tucker/canonical decomposition of the coefficients tensor $\mathbf{D}_\Lambda = [d_\Lambda(i_1, i_2, i_3)] \in \mathbb{R}^{n_1 \times n_2 \times n_3}$, $i_\ell \in \{1, \dots, n_\ell\}$, obtained by reshaping the diagonal of the matrix $\mathcal{F}_2(\Lambda) \in \mathbb{R}^{n^3 \times n^3}$ to the third order tensor \mathbf{D}_Λ . For example, in the case of discrete Laplacian the elements of the corresponding rank-3 coefficients tensor take a simple form

$$d_\Delta(i_1, i_2, i_3) = \lambda_{i_1} + \lambda_{i_2} + \lambda_{i_3},$$

with the eigenvalues λ_{i_ℓ} of univariate Laplacian.

For the ease of exposition, let us suppose that the 1D elliptic operators A_ℓ are all the same for three dimensions so that we omit the index ℓ in notations for $\lambda_i = \lambda_i^{(\ell)}$. Then the elements of the rank-3 coefficients tensor $\mathbf{D}_A = [d_A(i, j, k)] \in \mathbb{R}^{n \times n \times n}$, $i, j, k = 1, \dots, n$, corresponding to the factorization of the target matrix A in the eigenbasis, take a form

$$d_A(i, j, k) = \lambda_i + \lambda_j + \lambda_k,$$

where the eigenvalues λ_i , $i = 1, \dots, n$, are given by (3.6). Hence, we arrive at the explicit representation for the entries of

$$\mathbf{D}_\Lambda = \mathbf{D}_A^{-\alpha} + \mathbf{D}_A^\alpha, \quad (3.12)$$

as follows

$$d(i, j, k) = \frac{1}{(\lambda_i + \lambda_j + \lambda_k)^\alpha} + (\lambda_i + \lambda_j + \lambda_k)^\alpha. \quad (3.13)$$

Here we point out that the rank- R canonical approximation of the third order tensor \mathbf{D}_Λ is equivalent to the R -term Kronecker representation of the diagonal matrix $\mathcal{F}_2(\Lambda) \in \mathbb{R}^{n^3 \times n^3}$, due to the relation

$$\mathcal{F}_2(\Lambda) = \sum_{k=1}^R \text{diag}(\mathbf{u}_1^{(k)} \otimes \mathbf{u}_2^{(k)} \otimes \mathbf{u}_3^{(k)}),$$

where $\mathbf{u}_\ell^{(k)} \in \mathbb{R}^{n_\ell}$ are the skeleton vectors of the corresponding canonical decomposition of \mathbf{D}_Λ . This is straightforwardly translated to the respective R -term Kronecker representation

of the matrix valued function $\mathcal{F}_2(A)$ of interest

$$\begin{aligned}
\mathcal{F}_2(A) &= (G_1^T \otimes G_2^T \otimes G_3^T) \mathcal{F}_2(\Lambda) (G_1 \otimes G_2 \otimes G_3) \\
&= (G_1^T \otimes G_2^T \otimes G_3^T) \sum_{k=1}^R \text{diag}(\mathbf{u}_1^{(k)} \otimes \mathbf{u}_2^{(k)} \otimes \mathbf{u}_3^{(k)}) (G_1 \otimes G_2 \otimes G_3) \\
&= \sum_{k=1}^R (G_1^T \text{diag} \mathbf{u}_1^{(k)} G_1) \otimes (G_2^T \text{diag} \mathbf{u}_2^{(k)} G_2) \otimes (G_3^T \text{diag} \mathbf{u}_3^{(k)} G_3).
\end{aligned} \tag{3.14}$$

The representation (3.14) benefits from the linear scaling in d for both storage size and matrix-vector multiplication cost.

In turn, the low-rank canonical decomposition (approximation) of the tensor \mathbf{D}_Λ given by (3.13) is performed with the robust multigrid full-to-Tucker-to-canonical algorithm [36, 31] sketched in Appendix 1.

The existence of the accurate low-rank canonical approximation of the tensor \mathbf{D}_Λ can be analyzed separately for both summands in (3.12). For the term with negative fractional power $\mathbf{D}_A^{-\alpha}$ the Laplace integral transform representation (2.9) and the corresponding sinc quadrature approximation for the integral on the real axis (2.10) apply to the target tensor pointwise to obtain

$$\mathbf{D}_A^{-\alpha}[i_1, i_2, i_3] = \frac{1}{\Gamma(\alpha)} \int_0^\infty t^{\alpha-1} e^{-t\mathbf{D}_A} dt \approx \sum_{k=-M}^M \hat{c}_k t_k^{\alpha-1} e^{-t_k \mathbf{D}_A} = \sum_{k=-M}^M c_k \bigotimes_{\ell=1}^d e^{-t_k \lambda_{i_\ell}}. \tag{3.15}$$

Assume that the argument in the exponential in (3.15) varies in the fixed interval on the positive semi-axis, i.e. $0 < a_0 \leq \lambda_i + \lambda_j + \lambda_k \leq a_1 < \infty$, which is the case in our construction, then there is the quasi-optimal choice of the quadrature points t_k and weights c_k that ensures the exponentially fast convergence of the quadrature rule in the number of terms, $2M + 1$ [18, 23, 34]. Hence the number of separable terms, $R = 2M + 1$, that is the respective canonical rank, can be estimated by

$$R \leq C |\log \varepsilon|,$$

where $\varepsilon > 0$ is the accuracy threshold. The rank bound for the positive power of \mathbf{D}_A^α , $0 < \alpha < 1$, follows from the pointwise (Hadamard product) factorization

$$\mathbf{D}_A^\alpha = \mathbf{D}_A \cdot \mathbf{D}_A^{\alpha-1}, \quad \alpha - 1 < 0,$$

where \mathbf{D}_A is the rank-3 tensor, implying $\text{rank}(\mathbf{D}_A^\alpha) \leq 3R$.

3.5 Preconditioner in the low-rank Kronecker form

We propose and analyze the two different candidates for the efficient preconditioning of the matrix valued function $\mathcal{F}_2(A)$:

(A) The preconditioning matrix is constructed by using the tensor decomposition of $\mathcal{F}_3(\Delta)$ by using the Fourier based diagonalization of the discrete anisotropic Laplacian Δ in the similar way as in [24];

(B) Making use of the direct low K -rank approximation to the reciprocal matrix valued function

$$\mathcal{F}_3(A) = (A^\alpha + A^{-\alpha})^{-1},$$

where the target discrete elliptic operator (matrix) A is factorized in the eigenbasis of the univariate elliptic operators A_ℓ , $\ell = 1, \dots, 3$, with variable coefficients.

First, we recall some basic rank-structured decompositions for functions of the discrete Laplacian presented in [24]. The one-dimensional Laplace operator $\Delta_{(\ell)}$ has an eigenvalue decomposition in the Fourier basis, i. e.

$$\Delta_{(\ell)} = F_\ell^* \Lambda_{(\ell)} F_\ell.$$

In the case of homogeneous Dirichlet boundary conditions the matrix $F_\ell \in \mathbb{R}^{n \times n}$ defines the sin-Fourier transform and the diagonal matrix $\Lambda_{(\ell)} = \text{diag}\{\lambda_1^{(\ell)}, \dots, \lambda_n^{(\ell)}\}$ is composed of the eigenvalues of the univariate discrete Laplacian, $\lambda_k^{(\ell)}$, which are given by

$$\lambda_k = -\frac{4}{h_\ell^2} \sin^2 \left(\frac{\pi k}{2(n_\ell + 1)} \right) = -\frac{4}{h_\ell^2} \sin^2 \left(\frac{\pi k h_\ell}{2} \right).$$

Analogously to section 3.3, we can use the properties of the Kronecker product and rewrite the first summand in (3.3) as

$$\Delta_{(1)} \otimes I_2 \otimes I_3 = (F_1^* \otimes F_2^* \otimes F_3^*) (\Lambda_{(1)} \otimes I_2 \otimes I_3) (F_1 \otimes F_2 \otimes F_3).$$

Rewriting the other summands in the same style, we finally can write equation (3.3) as

$$\Delta = (F_1^* \otimes F_2^* \otimes F_3^*) (\Lambda_1 \otimes I_2 \otimes I_3 + I_1 \otimes \Lambda_2 \otimes I_3 + I_1 \otimes I_2 \otimes \Lambda_3) (F_1 \otimes F_2 \otimes F_3). \quad (3.16)$$

For $d = 2$, the expression simplifies to

$$\Delta = (F_1^* \otimes F_2^*) \underbrace{(\Lambda_1 \otimes I_2 + I_1 \otimes \Lambda_2)}_{=: \Lambda} (F_1 \otimes F_2). \quad (3.17)$$

With the help of the eigenvalue decomposition of Δ (3.17), we can compute a function $\mathcal{F} = \mathcal{F}_3$ applied to Δ as

$$\mathcal{F}(\Delta) = (F_1^* \otimes F_2^*) \mathcal{F}(\Lambda) (F_1 \otimes F_2).$$

Supposing low-rank decompositions for both $\mathcal{F}(A)$ and a vector $\mathbf{x} \in \mathbb{R}^N$ in the same style as in to section 3.3, we can compute a matrix-vector product as

$$\begin{aligned} \mathcal{F}(\Delta) \mathbf{x} &\approx (F_1^* \otimes F_2^*) \left(\sum_{k=1}^R \text{diag}(\mathbf{u}_1^{(k)} \otimes \mathbf{u}_2^{(k)}) \right) (F_1 \otimes F_2) \left(\sum_{j=1}^S \mathbf{x}_1^{(j)} \otimes \mathbf{x}_2^{(j)} \right) \\ &= \sum_{k=1}^R \sum_{j=1}^S F_1^* (\mathbf{u}_1^{(k)} \odot F_1 \mathbf{x}_1^{(j)}) \otimes F_2^* (\mathbf{u}_2^{(k)} \odot F_2 \mathbf{x}_2^{(j)}), \end{aligned} \quad (3.18)$$

where \odot denotes the componentwise (Hadamard) product.

Using the sin-FFT, expression (3.18) can be evaluated in the factored form in $\mathcal{O}(RSn \log n)$ flops, where $n = \max(n_1, n_2)$, and S is the Kronecker rank of vector \mathbf{x} .

For $d = 3$, with completely analogous reasoning, equation (3.18) becomes

$$\mathcal{F}(A)\mathbf{x} = \sum_{k=1}^R \sum_{j=1}^S F_1^*(\mathbf{u}_1^{(k)} \odot F_1 \mathbf{x}_1^{(j)}) \otimes F_2^*(\mathbf{u}_2^{(k)} \odot F_2 \mathbf{x}_2^{(j)}) \otimes F_3^*(\mathbf{u}_3^{(k)} \odot F_3 \mathbf{x}_3^{(j)}), \quad (3.19)$$

and similar in the case of $d > 3$. It can be evaluated in $\mathcal{O}(dRSn \log n)$ flops for K -rank structured vectors represented on $n^{\otimes d}$ Cartesian grid.

It is worth to note that the previous constructions remain valid also in the case of anisotropic Laplacian

$$\mathcal{B} = - \sum_{\ell=1}^d \frac{\partial}{dx_\ell} b^\ell \frac{\partial}{dx_\ell}, \quad \text{with some constants } b^\ell > 0. \quad (3.20)$$

In case (A), for the sake of preconditioning, we need the low K -rank approximation¹ to the matrix valued function of the form

$$\mathcal{F}_3(B) = (B^\alpha + B^{-\alpha})^{-1},$$

where the anisotropic Laplacian stiffness matrix B corresponding to the operator in (3.20) can be factorized in the Fourier basis as in (3.16). To that end, we define the average coefficients

$$b_0^\ell = \frac{1}{2}(\max a_\ell^+(x) + \min a_\ell^-(x)), \quad \ell = 1, 2, 3,$$

where $a_\ell^+(x) > 0$ and $a_\ell^-(x) > 0$ are chosen as *majorants and minorants* of the equation coefficient $a_\ell(x_\ell)$, respectively. Then we introduce the fractional anisotropic Laplacian type operator \mathcal{B} generated by the constant coefficients b_0^ℓ , $\ell = 1, 2, 3$, as follows

$$\mathcal{B}^\alpha := \left(- \sum_{\ell=1}^d \frac{\partial}{dx_\ell} b_0^\ell \frac{\partial}{dx_\ell} \right)^\alpha, \quad 0 \leq \alpha \leq 1, \quad (3.21)$$

and define the desired preconditioning matrix by using the discrete versions of the nonlocal operators \mathcal{B}^α and $\mathcal{B}^{-\alpha}$ in a form of a weighted sum of the matrix B^α and its inverse

$$B_0 = \beta B^{-\alpha} + \frac{\gamma}{\beta} B^\alpha. \quad (3.22)$$

It can be proven that the condition number of the preconditioned matrix $B_0^{-1} \mathcal{F}_2(A)$, where $\mathcal{F}_2(A) = \beta A^{-\alpha} + \frac{\gamma}{\beta} A^\alpha$, is uniformly bounded in n .

Theorem 3.2 *Let the matrix B_0 be given by (3.22). Under the above assumptions the condition number of the preconditioned matrix for the target Lagrange equation with the system matrix $\mathcal{F}_2(A)$ is uniformly bounded in n , specifically*

$$\text{cond}\{B_0^{-1} \mathcal{F}_2(A)\} \leq C \frac{\max\{(1+q)^\alpha, (1-q)^{-\alpha}\}}{\min\{(1+q)^{-\alpha}, (1-q)^\alpha\}}$$

with some constant $0 < q < 1$ independent on the grid size n .

¹Note that the numerical algorithm for the Tucker and canonical tensor decomposition of the d th-order tensors has been introduced in [36] and it was adapted to the case of fractional Laplacian in [24].

Proof. The matrix B generated by the coefficients b_0^ℓ corresponding to (3.21) allows the condition number estimate

$$\text{cond}\{B^{-1}A\} \leq C \frac{1+q}{1-q}, \quad \text{with} \quad q := \max_{\ell} \max_x \frac{a_{\ell}^{+}(x) - b_0^{\ell}}{b_0^{\ell}} < 1,$$

which is the consequence of the spectral equivalence estimate

$$C_0(1-q)B \leq A \leq C_1(1+q)B, \quad (3.23)$$

where the latter follows from the simple bounds

$$a_{\ell}^{+}(x) \leq (1+q)b_0^{\ell}, \quad (1-q)b_0^{\ell} \leq a_{\ell}^{-}(x), \quad \ell = 1, 2, 3.$$

As a result of (3.23), we readily derive the spectral bounds for the fractional elliptic operators of interest,

$$C_0(1-q)^{\alpha}B^{\alpha} \leq A^{\alpha} \leq C_1(1+q)^{\alpha}B^{\alpha},$$

and

$$C_0(1+q)^{-\alpha}B^{-\alpha} \leq A^{-\alpha} \leq C_1(1-q)^{-\alpha}B^{-\alpha}.$$

This proves the Theorem on the spectral equivalence of the preconditioner B_0 by summing up the above estimates with the proper weights. Indeed, we obtain for $\mathcal{F}_2(A) = \beta A^{-\alpha} + \frac{\gamma}{\beta} A^{\alpha}$

$$\mathcal{F}_2(A) \leq C_1(\beta(1-q)^{-\alpha}B^{-\alpha} + \frac{\gamma}{\beta}(1+q)^{\alpha}B^{\alpha}) \leq C_1 \max\{(1+q)^{\alpha}, (1-q)^{-\alpha}\}B_0,$$

and likewise

$$C_0 \min\{(1+q)^{-\alpha}, (1-q)^{\alpha}\}B_0 \leq C_0(\beta(1+q)^{-\alpha}B^{-\alpha} + \frac{\gamma}{\beta}(1-q)^{\alpha}B^{\alpha}) \leq \mathcal{F}_2(A),$$

which completes the proof. ■

The practical application of this Theorem in our numerical computations presupposes the low K -rank approximation of the matrix valued function of anisotropic Laplacian, B_0^{-1} , which is performed by using the multigrid Tucker approximation with the consequent Tucker-2-Canonical transform, applied to the respective diagonal core matrix $\mathcal{F}_2(A)$, see also §3.4 and Appendix 1.

To conclude the discussion of case (A) we notice that the presented preconditioning technique also applies to the case of degenerate elliptic operator with the non-negative equation coefficients $a_{\ell}(x_{\ell}) \geq 0$ for some spacial directions because the function $\lambda^{\alpha} + \lambda^{-\alpha} \geq \text{constant} > 0$ for all $\lambda \geq 0$.

In case (B), we perform the direct low K -rank tensor approximation of the matrix valued function $\mathcal{F}_3(A)$ along the same line as it is done for the target matrix function $\mathcal{F}_2(A)$ by using factorization in the eigen-basis of the univariate elliptic operators with variable coefficients, see also (3.14).

3.6 The PCG scheme with rank truncation

For operators `func` and `precond` given in a low-rank format, such as (3.10) (for $d = 2$) or (3.11) (for $d = 3$) and (3.18) (for $d = 2$) or (3.19) (for $d = 3$), respectively. Krylov subspace methods can be applied very efficiently, since they only require matrix-vector products.

In our applications, we use the formulation of the PCG method in Algorithm 1, [24], which is independent of d , as long as an appropriate rank truncation procedure `trunc` is chosen. As adaptive rank truncation procedure we use the reduced singular value decomposition in the case $d = 2$ and the reduced higher order singular value decomposition based on the Tucker-to-canonical approximation is used for $d = 3$, see Appendix 1 and [36] for details.

For the sake of completeness we present this algorithm in Appendix 2.

4 Numerical tests

In this section, we present numerical results for both the 2D and 3D cases. In all tests, we choose $\alpha = 1, 1/2, 1/10$, rank truncation parameter $\varepsilon = 10^{-6}$, the preconditioner rank $R = 6$, and $\beta = 1$. Throughout this section, let $A = A_h$ be the FDM discretization of the target elliptic operator \mathcal{A} . We investigate the numerical results and properties of the algorithm for solving equation (3.2),

$$(\beta A^{-\alpha} + \frac{\gamma}{\beta} A^\alpha) \mathbf{u} = \mathbf{y}_\Omega,$$

with respect to the optimal control \mathbf{u} and subsequently equation (3.1), that is

$$\mathbf{y} = \beta A^{-\alpha} \mathbf{u},$$

with respect to the state variable \mathbf{y} .

The PCG iteration is stopped when the relative residual is small enough, that is whenever

$$\left| \int_{\Omega} (\beta A^{-\alpha} + \frac{\gamma}{\beta} A^\alpha) \tilde{u} - y_\Omega \, dx \right| \leq 10^{-5}$$

holds for \tilde{u} solution of (2.4) discretized on the computational mesh. For the sake of simplicity, we define

$$A_u := (\beta A^{-\alpha} + \frac{\gamma}{\beta} A^\alpha).$$

Throughout our numerical tests, we consider the following right hand sides y_Ω : box-type and H -type shapes as shown in Figures 4.1 and 4.2 for 2D and 3D cases, respectively.

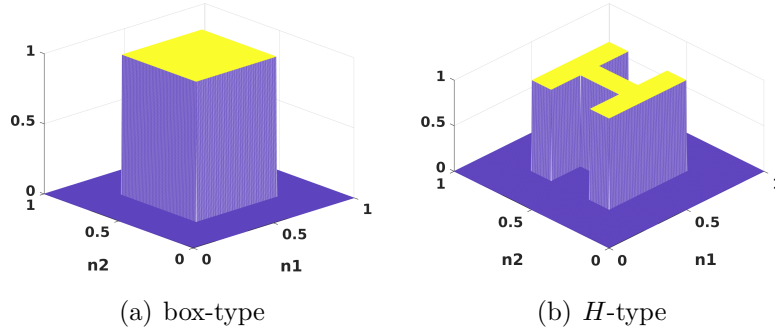


Figure 4.1: Box-type and H -form-type right hand sides y_Ω for the 2D control problem.

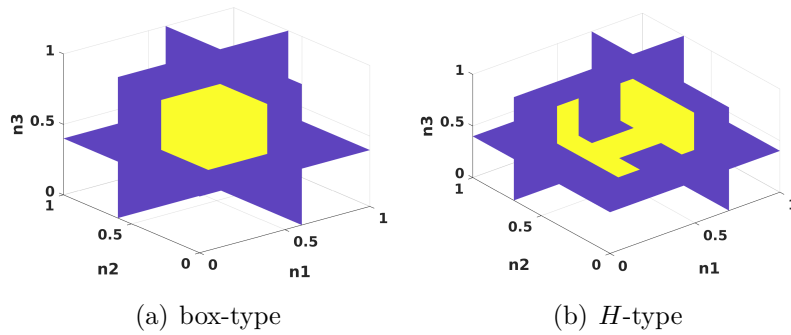


Figure 4.2: Box-type and H -form-type right hand sides y_Ω for the 3D control problem.

For solution of the control problem we use the partly high oscillating equation coefficients

$$a_1(x_1) = \sin(100\pi x_1) + 1.1, \quad (4.1)$$

$$a_2(x_2) = \sin(x_2) \cos(x_2), \quad (4.2)$$

$$a_3(x_3) = \cos(5\pi x_3) + 2 \quad (4.3)$$

for the construction of the diagonal equation coefficient matrices in a form (2.6) and (2.7) for the 2D and 3D cases, respectively.

In what follows, different preconditioning methods are used: in 2D case, we use an imprecise low K -rank approximation of the inverse matrix A_u^{-1} as a preconditioner, whereas in 3D case, the classical anisotropic Laplace operator in the low-rank Kronecker form is used as a preconditioner, see chapter 3.5, Theorem 3.2 and [24].

All simulations are performed in Matlab 2019b on a laptop with 16GB RAM and Intel(R) Core(TM) i7-8650U, using Ubuntu 18.04.

We use the low-rank canonical representation for the solution vector \mathbf{u} and for the right-hand side, and a short-term Kronecker product decomposition of all matrices involved. We maintain the quasi-optimal rank bound for the solution vector adapted to the given accuracy threshold. For the decomposition of the governing operators in 3D case we apply the multi-grid Tucker tensor approximation [36] and the subsequent Tucker-to-canonical transform.

The adaptive rank reduction for the rank-structured tensors representing the current iterant for the vector \mathbf{u} in the course of PCG iteration is calculated by the canonical-to-Tucker algorithm [35] combined with the Tucker-to-canonical transform. The basic tensor operations are performed by using the programs from the Matlab TESC package on tensor numerical methods developed in the recent years by the second and third authors, see [31] for short descriptions and related references.

4.1 Numerical tests for 2D case

First, we validate the usage of the tensor structured PCG algorithm by comparison with the backslash Matlab solver that is applied to the direct finite difference method discretization of equations (3.2) and (3.1) as well as by investigating the singular values of the involved operator A_u .

We also present the solutions for the optimal control \mathbf{u} and for the state variable \mathbf{y} in the respective equations (3.2) and (3.1) and investigate the impact of different regularization parameter values $\gamma = 1, 0.01$, and different fractional parameters α . Note that the preconditioning in 2D case is done by making use of the direct low-rank approximation to the reciprocal matrix valued function $\mathcal{F}_3(A)$, see section 3.5.

Table 4.1 shows the times needed by both the rank structured pcg solver and the backslash Matlab solver for solving equation

$$A^\alpha \mathbf{u} = \mathbf{y}_\Omega \quad (4.4)$$

for different grid sizes, the box-type design function and with a fixed parameter $\alpha = 1$. One can clearly observe that the rank structured pcg solver outperforms the full Matlab solver for a grid size $n \geq 128$.

Table 4.2 shows the times needed by the different solvers when considering equation (3.2) for a fixed grid size of $n = 64$ grid points in each dimension and different values for α as well as the time needed to set up the operator A_u as preliminary work for both solvers. Due to a lack of memory capacity, it is not possible to store the operator A_u in full size format for grid sizes with $n > 64$ grid points in each dimension, see section 4.2 for more details.

grid points	time pcg	time full solver
64	0,0079	0,0035
128	0,0145	0,0183
256	0,0306	0,0796
512	0,0454	0,4122
1024	0,0937	1,8072
2048	0,5994	8,5634

Table 4.1: Times in seconds needed by the rank-structured pcg scheme and the full-size scheme to solve (4.4) with different numbers of grid points and $\alpha = 1$.

Figure 4.3 shows the errors that occur for different α when using the rank structured solver compared to the full size solver for equation (3.2), which do not exceed an favourable error bound of 10^{-6} .

	$\alpha = 1$	$\alpha = 1/2$	$\alpha = 1/10$
time low-rank pcg	0.0092	0.0089	0.0051
time full solver	0.3583	0.4697	0.4847
time setting up operator (low-rank)	0.1097	0.0264	0.0422
time setting up operator (full)	1.1808	21.2779	22.5202

Table 4.2: Times for the rank-structured pcg solver and the full-size solver for solution of (3.2) with $n = 64$ grid points in each dimension and different α and times needed to set up A_u as preliminary work.

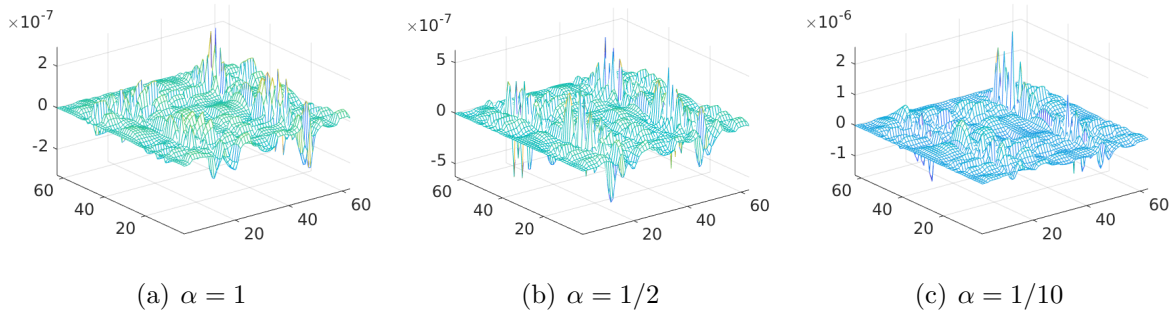


Figure 4.3: Error for the rank-structured solver solution compared to the full-size solver solution of (3.2), $n = 64$.

In order to validate the existence of the accurate low Kronecker-rank approximation to the operator A_u and its inverse,

$$A_{inv} = (A^\alpha + A^{-\alpha})^{-1},$$

which is required for preconditioning needs, we investigate the singular values of the corresponding matrices. Figure 4.4 demonstrates that for both operator cases A_u and A_{inv} and an exemplary grid size of 511 grid points in each dimension, there is an exponential decay of the corresponding singular values, which justifies the existence of an accurate low-rank representation.

In what follows, we investigate the time the pcg algorithm needs to solve (3.2),

$$A_u \mathbf{u} = \mathbf{y}_\Omega,$$

in our test setting. The corresponding tables and figures display the results for the box-type design function. Table 4.3 shows the number of iterations needed by the solver when considering different grid sizes and different values for α . The results validate a grid independence of the used pcg solver concerning the needed numbers of iterations.

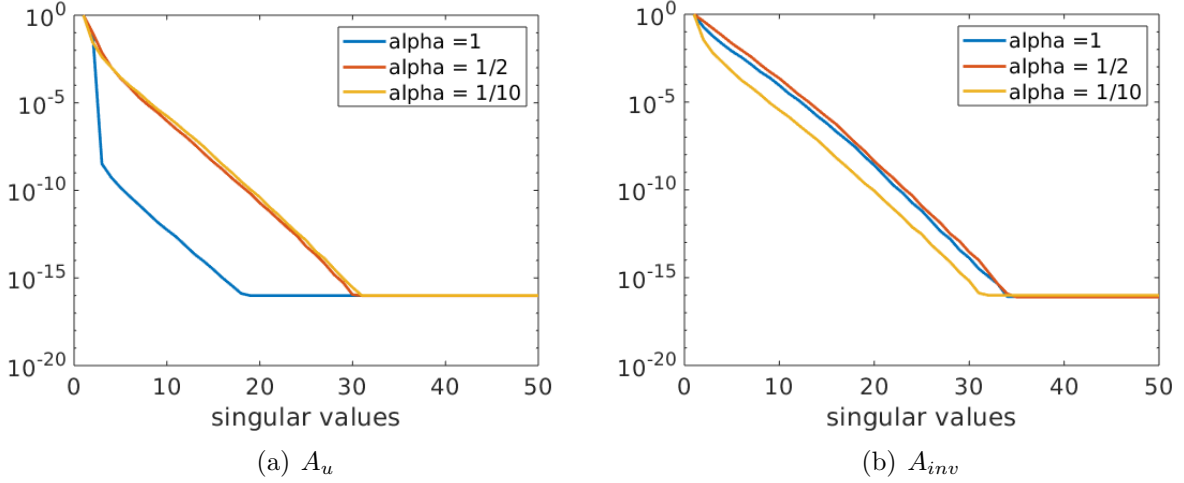


Figure 4.4: Decay of singular values for operators A_u and A_{inv} with different values of α and a univariate grid size with $n = 511$ grid points in each dimension.

grid points	$\alpha = 1$	$\alpha = 1/2$	$\alpha = 1/10$
64	2	2	1
128	2	2	2
256	2	2	2
512	2	2	2
1024	2	2	2
2048	3	2	2
4098	4	2	3
8196	4	3	3

Table 4.3: Number of iterations for the low-rank solver for solution of $(A^\alpha + A^{-\alpha})\mathbf{u} = \mathbf{y}_\Omega$ with different numbers of grid points and different values of α . The box-type design function is considered.

Figure 4.5 represents the time that the pcg algorithm needs for one iteration. The presented data validates the theoretical findings from section 3.3, that is the numerical cost for the algorithm of the order of $O(RSn^2)$. Therefore, the results demonstrate that the low-rank pcg scheme circumvents the curse of dimensionality.

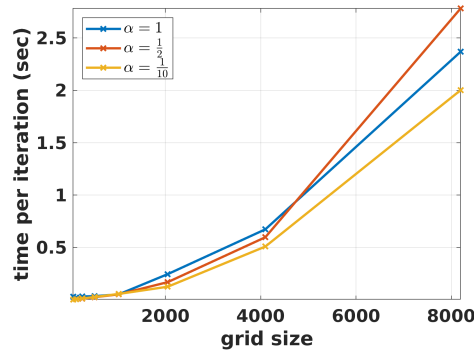


Figure 4.5: Times per iterations of PCG Algorithm for different grid sizes and different values of α considering the box-type design function.

4.1.1 Solution for optimal control

In this section, we present the solution for the optimal control \mathbf{u} , which means that with the help of the low-rank PCG algorithm, we solve equation (3.2),

$$A_u \mathbf{u} = (A^\alpha + A^{-\alpha}) \mathbf{u} = \mathbf{y}_\Omega.$$

Figures 4.6 - 4.8 show the solutions computed by the rank-structured PCG scheme using the coefficients functions (4.1) and (4.2), different right hand sides \mathbf{y}_Ω , fractional exponents α , and a grid of size $n = 255$ grid points in each dimension. In figures 4.6 and 4.7 we consider $\gamma = 1$, whereas in figure 4.8, we investigate the impact of a small regularization parameter $\gamma = 0.01$.

The effect of the highly oscillating coefficient test function (4.1) on the structure of the optimal control \mathbf{u} can be recognized in all figures.

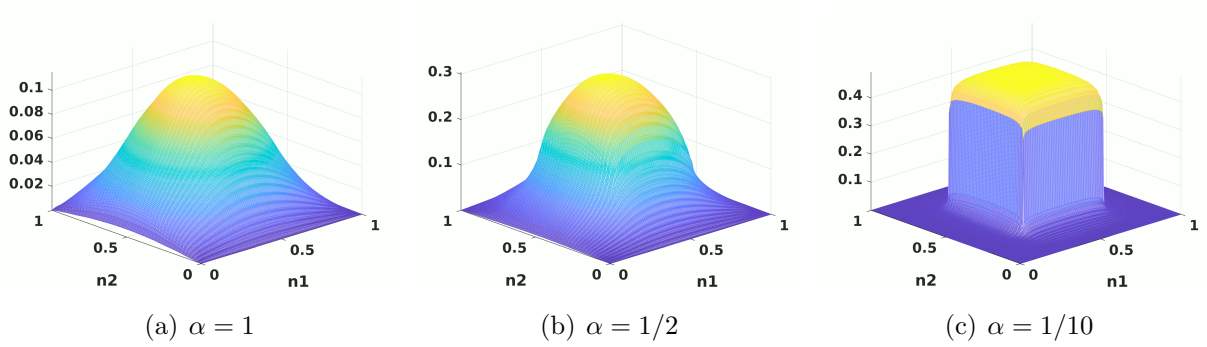


Figure 4.6: Impact of fractional exponent α on solutions \mathbf{u} of (3.2) for box-type right hand side \mathbf{y}_Ω , $\gamma = 1$.

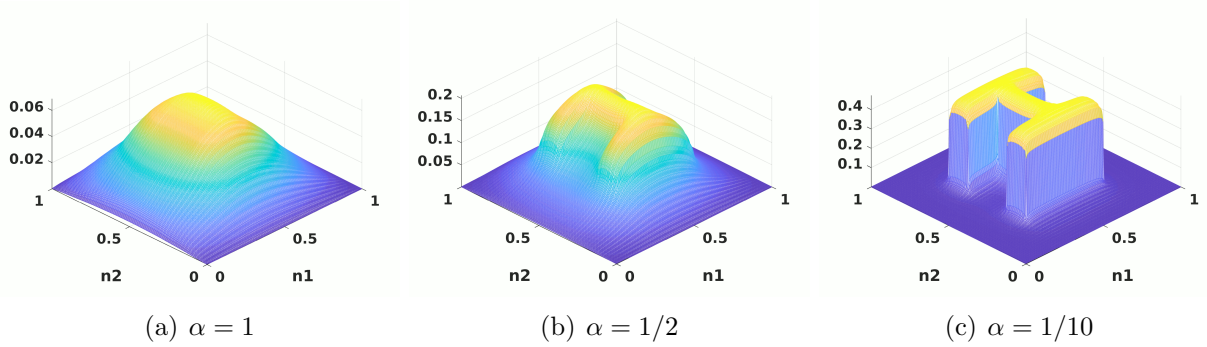


Figure 4.7: Impact of fractional exponent α on solutions \mathbf{u} of (3.2) for H -type right hand side \mathbf{y}_Ω , $\gamma = 1$.

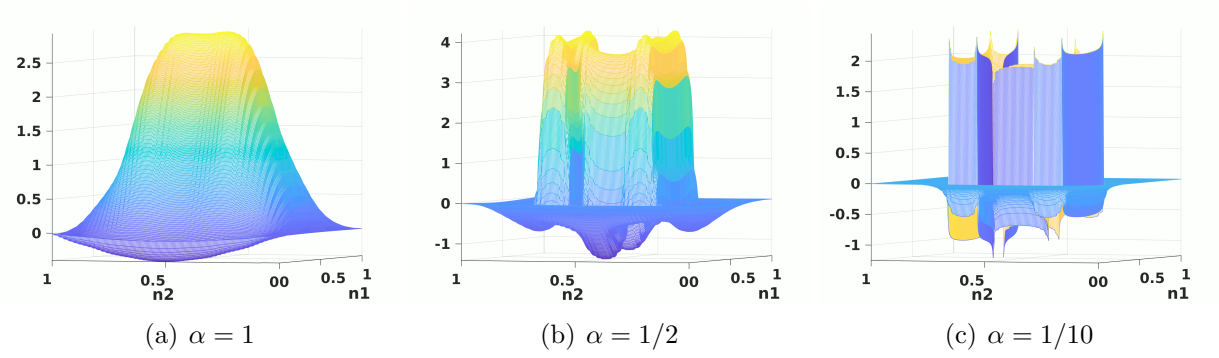


Figure 4.8: Impact of small regularization parameter $\gamma = 0.01$ on solutions \mathbf{u} for H -type design function \mathbf{y}_Ω and different values for α .

4.1.2 Solution for State Variable

In this section, the solution for the state variable \mathbf{y} is presented, that is we solve equation (3.1),

$$\mathbf{y} = A^{-\alpha} \mathbf{u},$$

where \mathbf{u} is the solution of (3.2) presented in section 4.1.1. Analogously, we consider the grid size $n = 255$ and compare the effects of different fractional exponents α and regularization parameter values $\gamma = 1$ (figures 4.9 and 4.10) and $\gamma = 0.01$ (figure 4.11).

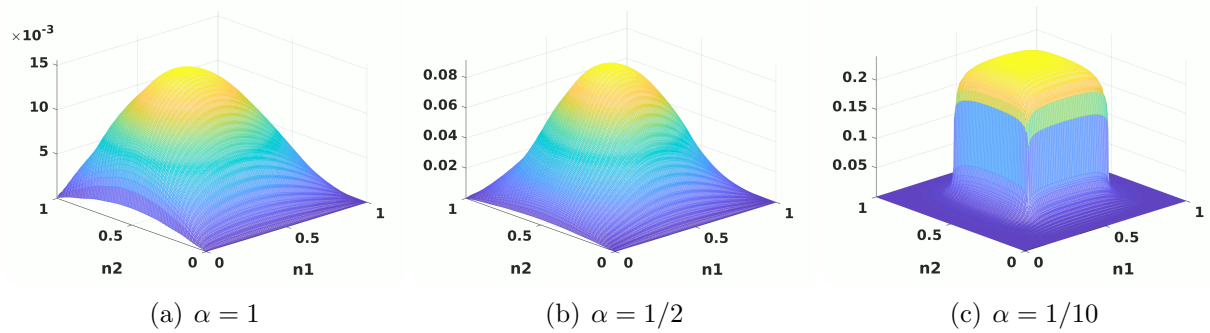


Figure 4.9: Impact of fractional exponent α on solutions \mathbf{y} of (3.1) for box-type right hand side \mathbf{y}_Ω , $\gamma = 1$.

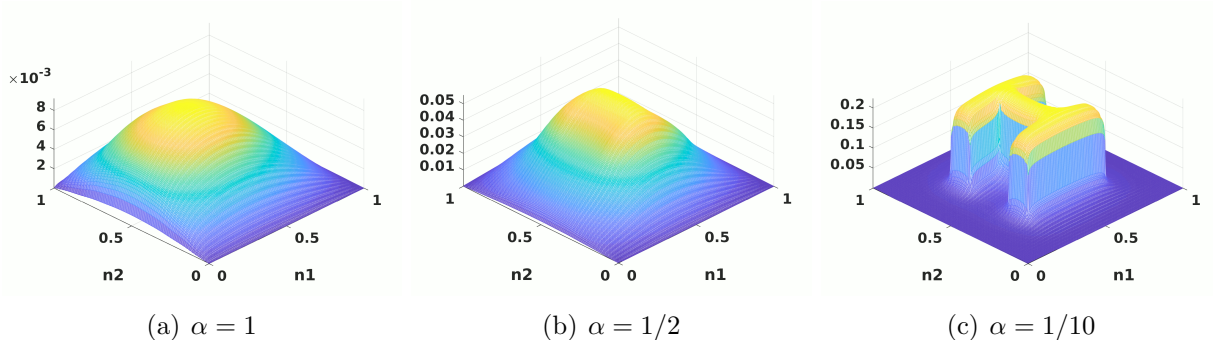


Figure 4.10: Impact of fractional exponent α on solutions \mathbf{y} of (3.1) for H -type right hand side \mathbf{y}_Ω , $\gamma = 1$.

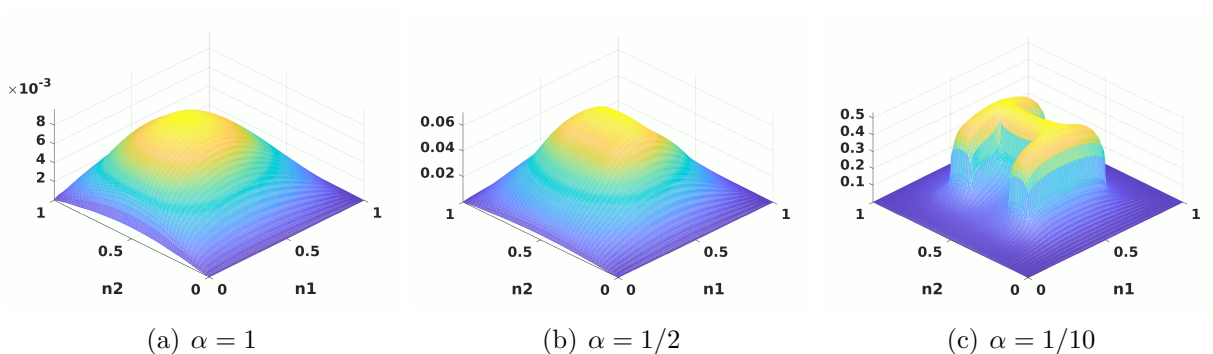


Figure 4.11: Impact of small regularization parameter $\gamma = 0.01$ on solutions \mathbf{y} for H -type design function \mathbf{y}_Ω and different values for α .

4.2 Numerical tests for 3D case

In this section the numerical results for the 3D case are presented. We first consider the computational time and then discuss the storage complexity of the algorithm. Further, we present 3D solutions for equations (3.2) and (3.1), that is the results of the numerical simulations for the optimal control \mathbf{u} and the state \mathbf{y} , respectively. In these calculations, we use a grid size of $n = 127$ grid points in each dimension, the regularization parameter $\gamma = 1$, and different values for $\alpha = 1, 1/2, 1/10$. As stated previously, we use the operator $(\Delta^\alpha + \Delta^{-\alpha})^{-1}$ in a low-rank format as preconditioning operator, where Δ is the classic negative Laplace operator (see section 3.5 for details).

4.2.1 Complexity results

First, we investigate the time the low-rank pcg scheme needs to solve equation (3.2),

$$(A^\alpha + A^{-\alpha})\mathbf{u} = \mathbf{y}_\Omega$$

for the H -type right hand side \mathbf{y}_Ω .

Table 4.4 shows the resulting computational times (in seconds) the pcg algorithm needs in total to solve (3.2), considering different numbers of grid points, different values for α and aforementioned coefficient functions (4.1) – (4.3).

Figure 4.12 represents the corresponding time per iteration in the presented test, resulting from tables 4.4 and 4.5. The presented data confirms the computational complexity of $O(RSn^2)$ (see section 3.3) and therefore proves that the used low-rank structures within the pcg scheme contribute to circumventing the course of dimensionality efficiently.

grid points	$\alpha = 1$	$\alpha = 1/2$	$\alpha = 1/10$
64	28.1	16.0	2.53
128	92.8	43.7	7.15
256	318.0	125.0	22.5
512	1180.0	512.0	66.8

Table 4.4: Times in seconds needed by the rank-structured solver to solve $(A^\alpha + A^{-\alpha})\mathbf{u} = \mathbf{y}_\Omega$ with different numbers of grid points and different values α . The H -type design function is considered.

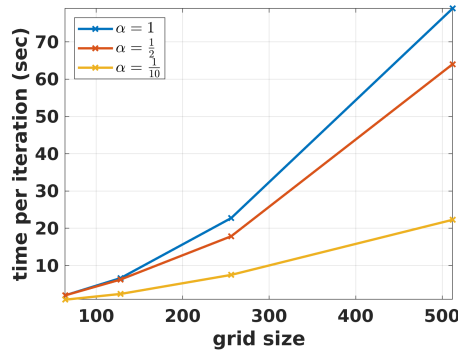


Figure 4.12: Times per iterations of the pcg algorithm for different grid sizes and different values of α considering the H -type design function.

Table 4.5 shows the number of iterations the algorithm needs to solve equation (3.2) for different numbers of grid points as well as different values for α . Analogously to the 2D case, the data verifies that the algorithm provides a solution scheme for the investigated problem class whose number of iterations is independent of the number of grid points.

grid points	$\alpha = 1$	$\alpha = 1/2$	$\alpha = 1/10$
64	14	8	3
128	14	7	3
256	14	7	3
512	15	8	3

Table 4.5: Numbers of iterations for the low-rank solver for solution of $(A^\alpha + A^{-\alpha})\mathbf{u} = \mathbf{y}_\Omega$ with different numbers of grid points and different values of α . The H -type design function is considered.

4.2.2 Effects of anisotropic preconditioning

In our tests, we use coefficient functions $a_1(x_1)$, $a_2(x_2)$, and $a_3(x_3)$ as defined in (4.1) – (4.3). As stated in Theorem 3.2, the condition number of the preconditioned operator is estimated

with the help of majorants and minorants of the coefficient functions involved in the problem. In our numerical test, the minorant corresponding to the coefficient function $a_2(x_2)$ tends to be zero, which then might lead to a unfavorable condition tending to infinity (see condition estimate in section 3.5). However, our numerical tests do not suffer from this fact, as the inverse term in operator A_u regularizes the spectrum. Nevertheless, we define a modified coefficient

$$\tilde{a}_2 := a_2 + 0.1$$

in order to change our numerical test slightly (which also circumvents any problems that might arise due to a bad condition) and to see the effects on the time complexity for solving equation (3.2). We also test the effect of using the anisotropic Laplacian (3.21),

$$B_0 = \beta B^{-\alpha} + \frac{\gamma}{\beta} B^{\alpha},$$

where B is the discretization of $\mathcal{B} := -\sum_{\ell=1}^d \frac{\partial}{\partial x_{\ell}} b_0^{\ell} \frac{\partial}{\partial x_{\ell}}$, used as preconditioning operator instead of the classic Laplacian. During the test, we use coefficient functions a_1, \tilde{a}_2 , and a_3 and choose

$$b_0^{\ell} = \frac{1}{2}(\max a_{\ell}(x) + \min a_{\ell}(x)), \quad \ell = 1, 2, 3, \quad (4.5)$$

as scaling constant coefficients.

Table 4.6 shows the results of both tests: The left table represents the number of iterations needed by the pcg scheme for solving (3.2) when using the same setting as in section 4.2.1 but replacing a_2 by \tilde{a}_2 . Note that the number of iterations can be reduced for $\alpha = 1$ and $\alpha = 1/2$.

The right table shows the number of iterations for the same setting as in section 4.2.1 but replacing a_2 by \tilde{a}_2 and using the anisotropic Laplacian (3.21) with coefficients defined in (4.5) as preconditioner. Again the number of iterations needed to solve (3.2) decreases for $\alpha = 1$ and $\alpha = 1/2$.

In both cases, we notice an improvement concerning the time complexity and still observe a grid independent number of iterations in order to solve the problem.

grid points	$\alpha = 1$	$\alpha = 1/2$	$\alpha = 1/10$
64	11	7	3
128	11	6	3
256	11	6	3
512	11	6	3

grid points	$\alpha = 1$	$\alpha = 1/2$	$\alpha = 1/10$
64	9	6	3
128	8	6	3
256	8	6	3
512	9	5	3

Table 4.6: Numbers of iterations for the low-rank solver for solution of $(A^{\alpha} + A^{-\alpha})\mathbf{u} = \mathbf{y}_{\Omega}$. *Left:* coefficient functions a_1, \tilde{a}_2 , and a_3 , classic Laplacian as preconditioner. *Right:* coefficient functions a_1, \tilde{a}_2 , and a_3 , anisotropic Laplacian as preconditioner. The H -type design function is considered

Remark 4.1 *From above tables concerning the time complexity, we observe that equation (3.2) can be solved fastest for small $\alpha \rightarrow 0$. This effect is due to the fact that for small values for α , both the operators A^{α} and $A^{-\alpha}$ approach the Identity matrix \mathbf{I} , so that ultimately only an equation similar to $\mathbf{I}\mathbf{u} = \mathbf{y}_{\Omega}$ has to be solved.*

It is worth to note that in 3D case the main bottleneck for the numerical treatment of nonlocal operators is the dramatic storage growth for the corresponding fully populated $n^3 \times n^3$ stiffness matrices as the volume size n^3 of the discretization grid increases. To point out further advantages of our low-rank scheme compared to a full format algorithm, we investigate the costs for storing the operator A of type (3.3) as well as for computing and storing the fractional operators A^α and $A^{-\alpha}$ in both a low-rank format and a full format. Figure 4.13 shows the respective required storage to store the discrete operator A for both tests.

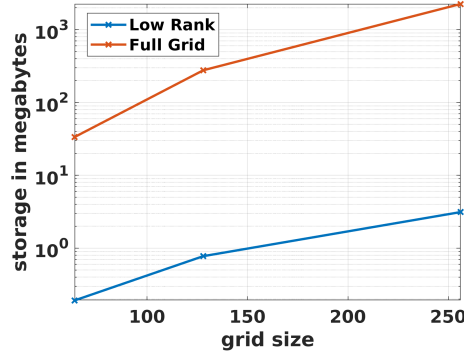


Figure 4.13: Storage complexity needed to store operator A when using a full format scheme and when using the low-rank scheme.

If we worked with the full format tensor in the given problem, we would have to store a tensor (matrix) of size $n^d \times n^d$ which means we would end up with a polynomial storage scaling in the number of grid points, which can only be handled by saving the operator in a sparse format. However, in order to compute A^α and its inverse $A^{-\alpha}$, the full format tensor is needed. As a consequence, their computations in our test exceed the storage capacity of the used laptop (16GB RAM) for $n \geq 32$ grid points in each dimension. As a result, the problem cannot be solved in a full format scheme with large grids.

However, in low-rank format we follow the computation and storage scheme presented in chapter 3.3, that is we compute a factorized form (3.8) of A^α and $A^{-\alpha}$ with the help of the eigenvalue decomposition. Thereafter, we compute $\mathcal{F}(\Lambda)$ in a canonical format (3.9) that has a computational cost of order $O(n^d)$, but only has to be computed once before the algorithm starts. Finally, we end up with a storage cost for the canonical format of order $O(dRn)$ which is only linear in the number of grid points.

All in all we stress that the given problem can only be solved with controllable precision by efficiently using low-rank structures of the involved operators.

4.2.3 Solutions for optimal control

Figures 4.14 and 4.15 show the solution for the control \mathbf{u} of equation (3.2),

$$A_u \mathbf{u} = \mathbf{y}_\Omega,$$

that is computed by the pcg scheme for two different right hand sides \mathbf{y}_Ω . We consider a grid size of $n = 127$ grid points in each dimension, regularization parameter $\gamma = 1$, and

different values for $\alpha = 1, 1/2, 1/10$.

Each figure shows slice planes for the volumetric (tensor) data \mathbf{u} , where the values in \mathbf{u} determine the contour colors. We choose three slice planes, where each of them is orthogonal to one dimension. Every slice plane could also be depicted analogously to the 2D figures in Figure 4.11.

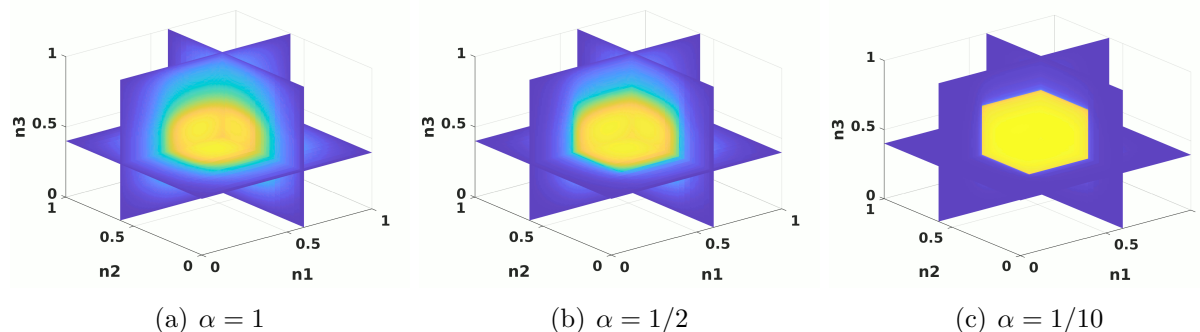


Figure 4.14: Impact of fractional exponent α on solutions \mathbf{u} of (3.2) for box-type right hand side \mathbf{y}_Ω and $n = 127$ grid points in each dimension.

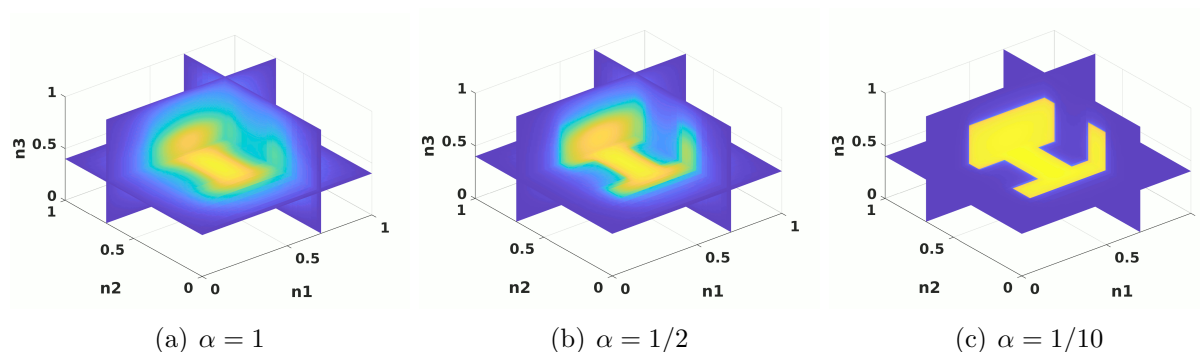


Figure 4.15: Impact of fractional exponent α on solutions \mathbf{u} of (3.2) for H -type right hand side \mathbf{y}_Ω and $n = 127$ grid points in each dimension.

Figure 4.16 visualizes in volumetric style the same data as in figure 4.15 for the case of H -typed right hand side \mathbf{y}_Ω .

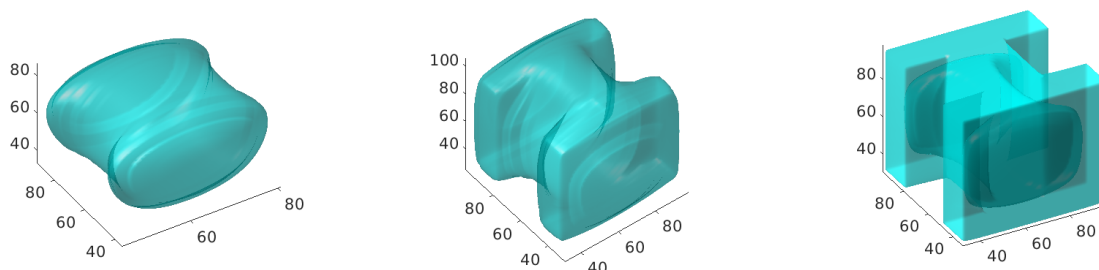


Figure 4.16: Volumetric visualization for the case of H -type: Impact of fractional exponent α on solutions \mathbf{u} of (3.2) for H -typed right hand side \mathbf{y}_Ω , see Fig. 4.15.

4.2.4 Solutions for state variable

Figures 4.17 and 4.18 represent the solution for the state \mathbf{y} of (3.1),

$$A^{-\alpha} \mathbf{u} = \mathbf{y},$$

where \mathbf{u} is the solution of (3.2) presented in section 4.2.3. Again we consider the grid size $n = 127$ and compare the effects of different fractional exponents α .

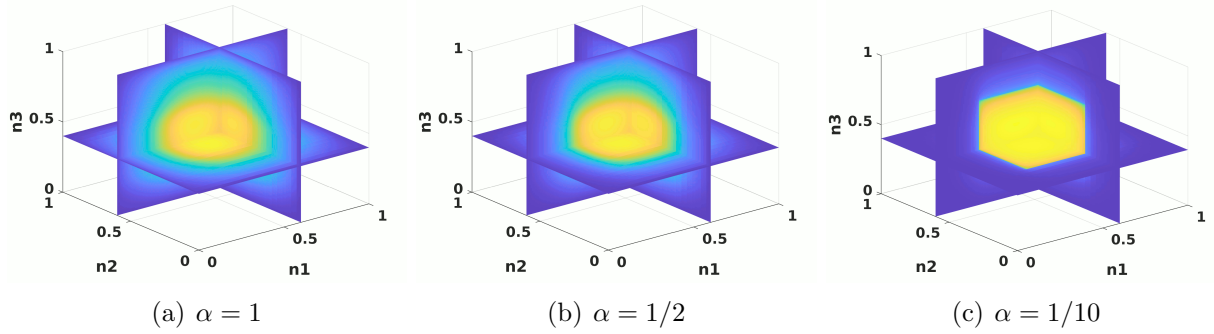


Figure 4.17: Impact of fractional exponent α on solutions \mathbf{y} of (3.1) for box-type right hand side \mathbf{y}_Ω , $\gamma = 1$ and $n = 127$ grid points in each dimension.

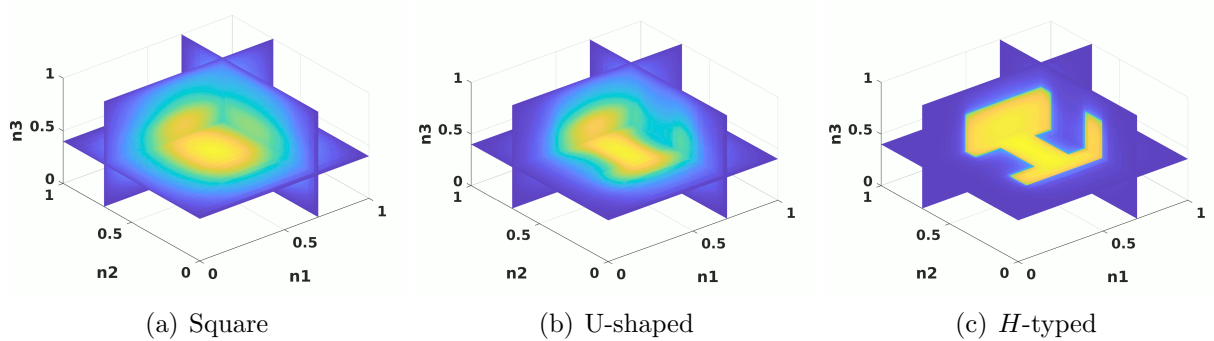


Figure 4.18: Impact of fractional exponent α on solutions \mathbf{y} of (3.1) for H -typed right hand side \mathbf{y}_Ω , $\gamma = 1$ and $n = 127$ grid points in each dimension.

5 Conclusions

We have introduced and analyzed a tensor numerical pcg scheme with adaptive rank truncation for the solution of optimal control problems constrained by fractional 2D and 3D elliptic Laplacian-type operators with variable separable coefficients, which essentially generalizes the results in [24]. To that end, we first have provided the theoretical solution setting by exploiting the separable structure of the involved functions of an elliptic operator and by deriving the corresponding finite difference discretization scheme on $n \times n \times n$ Cartesian grids. With the help of the eigenvalue decomposition of the one-dimensional differential operators and using the efficient Tucker-to-canonical tensor approximation techniques, we have

managed to present the fully populated stiffness matrix in factorized low-rank format. For preconditioning, we have extended the low-rank structures for the classic Laplace operator developed in [24] to the case of anisotropic Laplacian in 3D.

As a result, we achieved a dimensionally independent quadratic complexity scaling in the number of univariate grid points, $O(RSn^2)$, for the (factorized) matrix-vector multiplication that also represents an upper bound for the complexity of the PCG solution scheme with rank truncation as a whole. Here R and S are, respectively, the (low) Kronecker ranks of the nonlocal solution operator (matrix) and the iterated unknown solution vector.

In our numerical study, we have verified the efficiency of our solution scheme over rank structured “data manifold” by comparison to the Matlab intern pcg routine and justified the existence of low-rank representations of the involved operators by investigating the decay of the respective singular values. Furthermore, in our numerical tests we have verified the computational cost of $O(RSn^2)$ for $d = 2, 3$ and have pointed out that the required memory capacity for solving the problem for large grids can only be handled by using the proposed low-rank method.

The presented approach can also be applied to the simpler case of control problems constraint via both classic and fractional Laplace operator. In order to reduce the numerical complexity further, the application of quantized tensor train formats to the involved operators and vectors may be examined. What is more, the effects of considering fractional operators with general rank- R separable coefficients may be investigated and analyzed.

Appendix 1: Short sketch on tensor numerical methods

Recent tensor numerical methods emerged as bridging of the basic tensor decompositions and algorithms of the multilinear algebra with the rigorous results in approximation theory on the low-rank representation of the multivariate functions and operators [18, 23]. The latter results on tensor-product approximation to multi-dimensional nonlocal operators have been first originated in the framework of the low-rank \mathcal{H} -matrix techniques [22].

The basic tensor decompositions used in multilinear algebra for the low-rank representation of the multidimensional tensors are the canonical [29] and Tucker [44] tensor formats.

For a tensor of order d given in a full size format

$$\mathbf{T} = [t_{i_1, \dots, i_d}] \in \mathbb{R}^{n_1 \times \dots \times n_d} \quad \text{with} \quad i_\ell \in I_\ell := \{1, \dots, n_\ell\}.$$

all operations scale exponentially with the dimension size, as $O(n^d)$ (assuming $n_\ell = n$). The so-called “curse of dimensionality” can be reduced or eliminated when the tensor is given in a rank-structured representation. A tensor in the R -term canonical format is defined by a sum of rank-1 tensors

$$\mathbf{T} = \sum_{k=1}^R \xi_k \mathbf{u}_k^{(1)} \otimes \dots \otimes \mathbf{u}_k^{(d)}, \quad \xi_k \in \mathbb{R}, \quad (5.1)$$

where $\mathbf{u}_k^{(\ell)} \in \mathbb{R}^{n_\ell}$ are normalized vectors, and R is the canonical rank. The storage cost of this parametrization is bounded by dRn . However, for $d \geq 3$, there is lack of stable algorithms to compute the canonical low-rank representation of a general tensor \mathbf{T} , that is, with the minimal number R in representation (5.1), and the respective decomposition with

the polynomial cost in d , i.e., the computation of the canonical decomposition is in general an N - P hard problem.

The Tucker tensor format is suitable for stable numerical decompositions with a fixed truncation threshold. We say that the tensor \mathbf{T} is represented in the rank- \mathbf{r} orthogonal Tucker format with the rank parameter $\mathbf{r} = (r_1, \dots, r_d)$ if

$$\mathbf{T} = \sum_{\nu_1=1}^{r_1} \dots \sum_{\nu_d=1}^{r_d} \beta_{\nu_1, \dots, \nu_d} \mathbf{v}_{\nu_1}^{(1)} \otimes \mathbf{v}_{\nu_2}^{(2)} \dots \otimes \mathbf{v}_{\nu_d}^{(d)},$$

where $\{\mathbf{v}_{\nu_\ell}^{(\ell)}\}_{\nu_\ell=1}^{r_\ell} \in \mathbb{R}^{n_\ell}$, $\ell = 1, \dots, d$ represents a set of orthonormal vectors and $\boldsymbol{\beta} = [\beta_{\nu_1, \dots, \nu_d}] \in \mathbb{R}^{r_1 \times \dots \times r_d}$ is the Tucker core tensor. However, the complexity of the Tucker tensor decomposition algorithm [12] is $O(n^{d+1})$ and it requires the tensor in full size format. This step is called the higher order singular value decomposition (HOSVD).

These tensor decompositions yield rank-structured representation of tensors (for $d = 2$ these are rank-structured matrices), which provide the reduction of the operations with tensor to one-dimensional operations. Given two tensors in the canonical tensor format,

$$\mathbf{A}_1 = \sum_{k=1}^{R_1} c_k \mathbf{u}_k^{(1)} \otimes \dots \otimes \mathbf{u}_k^{(d)}, \quad \mathbf{A}_2 = \sum_{m=1}^{R_2} b_m \mathbf{v}_m^{(1)} \otimes \dots \otimes \mathbf{v}_m^{(d)}.$$

the Euclidean scalar product

$$\langle \mathbf{A}_1, \mathbf{A}_2 \rangle := \sum_{k=1}^{R_1} \sum_{m=1}^{R_2} c_k b_m \prod_{\ell=1}^d \langle \mathbf{u}_k^{(\ell)}, \mathbf{v}_m^{(\ell)} \rangle,$$

and Hadamard product of tensors $\mathbf{A}_1, \mathbf{A}_2$,

$$\mathbf{A}_1 \odot \mathbf{A}_2 := \sum_{k=1}^{R_1} \sum_{m=1}^{R_2} c_k b_m \left(\mathbf{u}_k^{(1)} \odot \mathbf{v}_m^{(1)} \right) \otimes \dots \otimes \left(\mathbf{u}_k^{(d)} \odot \mathbf{v}_m^{(d)} \right).$$

are computed in $O(dR_1R_2n)$ complexity. The rank of the resulting tensor is a product of the original ranks of tensors.

In multilinear algebra the Tucker tensor decomposition was used in chemometrics, psychometrics, and signal processing for the quantitative analysis of the experimental data, without special demands on accuracy and data size. These techniques could not be applied for the usage in numerical analysis of PDEs, with large data arrays and high accuracy requirements. Also, for general type tensors given in the rank- R canonical format, with large ranks and with large mode size n , both construction of the full size tensor representation and HOSVD become intractable.

However, it was found in [32] that for function related tensors the Tucker tensor decomposition exhibits exceptional approximation properties. In particular, it was proven and demonstrated numerically that for a class of higher order tensors arising from the discretization of linear operators and functions in \mathbb{R}^d using $n \times n \dots \times n$ Cartesian grids the approximation error of the Tucker decomposition decays exponentially in the Tucker rank [32, 35]. These findings motivated introducing the multigrid Tucker tensor decomposition

[36] which is used in this paper to transform the reshaped discretized elliptic operators, being the fully populated 3D tensors, into the low-rank canonical tensors. The main advantage of the multigrid Tucker decomposition is the elimination of the HOSVD for large grids, thus reducing the required storage to the maximum size of the tensor, $O(n^d)$, instead of $O(n^{d+1})$. The last step in the transformation of the full tensor to canonical format is performed by using the Tucker-to-canonical algorithm [31].

Main motivation for tensor numerical methods in scientific computing was the invention of the canonical-to-Tucker (C2T) decomposition and the reduced HOSVD (RHOSVD) (introduced in [36], see detailed description in [31, 34]) which does not require the construction of a full size tensor. The complexity of the RHOSVD is $O(dn^2R)$, where R is the canonical rank, and it applies to any dimension size d .

Tensor operations with canonical tensors, provide an advantage of one-dimensional complexity of d -dimensional operations. However, these operations lead to “curse of ranks”, since the ranks are multiplied and after several operations calculations become intractable. The C2T transform provides a robust tool for the rank reduction of the canonical tensors. The combination of C2T algorithm with the Tucker-to-canonical transform² is the main working horse in all rank-truncation procedures. In this paper, these transforms are used to reduce the ranks of the involved quantities in the course of PCG iteration for the numerical solution of the 3D control problems with fractional elliptic operators in constraints.

Appendix 2: Precoditioned CG iteration in low-rank tensor formats

As the rank truncation procedure, in our implementation we apply the reduced SVD algorithm in 2D case and the RHOSVD based canonical-to-Tucker-to-canonical algorithm (see [36]) as described in Section 5.

Acknowledgment

This research has been supported by the German Research Foundation (DFG) within the *Research Training Group 2126: Algorithmic Optimization*, Department of Mathematics, University of Trier, Germany.

References

- [1] G. Allaire. *Numerical analysis and optimization: an introduction to mathematical modelling and numerical simulation*. Oxford University Press, 2007.

²This decomposition applies to a small size core tensor for the mixed Tucker-canonical format of type

$$\mathbf{T}_{(\mathbf{r})} = \left(\sum_{k=1}^R b_k \mathbf{u}_k^{(1)} \otimes \dots \otimes \mathbf{u}_k^{(d)} \right) \times_1 V^{(1)} \times_2 V^{(2)} \times_3 \dots \times_d V^{(d)},$$

providing the canonical tensor rank of the order of $R \leq r^2$ in 3D case [31].

Algorithm 1 Preconditioned CG method in low-rank format

Input: Rank truncation procedure `trunc`, rank tolerance parameter ε , linear function in low-rank format `fun`, preconditioner in low-rank format `precond`, right-hand side tensor \mathbf{B} , initial guess $\mathbf{X}^{(0)}$, maximal iteration number k_{\max}

```
1:  $\mathbf{R}^{(0)} \leftarrow \mathbf{B} - \text{fun}(\mathbf{X}^{(0)})$ 
2:  $\mathbf{Z}^{(0)} \leftarrow \text{precond}(\mathbf{R}^{(0)})$ 
3:  $\mathbf{Z}^{(0)} \leftarrow \text{trunc}(\mathbf{Z}^{(0)}, \varepsilon)$ 
4:  $\mathbf{P}^{(0)} \leftarrow (\mathbf{Z}^{(0)})$ 
5:  $k \leftarrow 0$ 
6: repeat
7:    $\mathbf{S}^{(k)} \leftarrow \text{fun}(\mathbf{P}^{(k)})$ 
8:    $\mathbf{S}^{(k)} \leftarrow \text{trunc}(\mathbf{S}^{(k)}, \varepsilon)$ 
9:    $\alpha_k \leftarrow \frac{\langle \mathbf{R}^{(k)}, \mathbf{Z}^{(k)} \rangle}{\langle \mathbf{P}^{(k)}, \mathbf{S}^{(k)} \rangle}$ 
10:   $\mathbf{X}^{(k+1)} \leftarrow \mathbf{X}^{(k)} + \alpha_k \mathbf{P}^{(k)}$ 
11:   $\mathbf{X}^{(k+1)} \leftarrow \text{trunc}(\mathbf{X}^{(k+1)}, \varepsilon)$ 
12:   $\mathbf{R}^{(k+1)} \leftarrow \mathbf{R}^{(k)} - \alpha_k \mathbf{S}^{(k)}$ 
13:   $\mathbf{R}^{(k+1)} \leftarrow \text{trunc}(\mathbf{R}^{(k+1)}, \varepsilon)$ 
14:  if  $\mathbf{R}^{(k+1)}$  is sufficiently small then
15:    return  $\mathbf{X}^{(k+1)}$ 
16:    break
17:  end if
18:   $\mathbf{Z}^{(k+1)} \leftarrow \text{precond}(\mathbf{R}^{(k+1)})$ 
19:   $\mathbf{Z}^{(k+1)} \leftarrow \text{trunc}(\mathbf{Z}^{(k+1)}, \varepsilon)$ 
20:   $\beta_k \leftarrow \frac{\langle \mathbf{R}^{(k+1)}, \mathbf{Z}^{(k+1)} \rangle}{\langle \mathbf{Z}^{(k)}, \mathbf{R}^{(k)} \rangle}$ 
21:   $\mathbf{P}^{(k+1)} \leftarrow \mathbf{Z}^{(k+1)} + \beta_k \mathbf{P}^{(k)}$ 
22:   $\mathbf{P}^{(k+1)} \leftarrow \text{trunc}(\mathbf{P}^{(k+1)}, \varepsilon)$ 
23:   $k \leftarrow k + 1$ 
24: until  $k = k_{\max}$ 
Output: Solution  $\mathbf{X}$  of  $\text{fun}(\mathbf{X}) = \mathbf{B}$ 
```

- [2] H. Antil and E. Otárola. *A FEM for an Optimal Control Problem of Fractional Powers of Elliptic Operators*. SIAM J. Control Optim., 53(6), pp.343-3456, 2015.
- [3] T. M. Atanackovic, S. Pilipovic, B. Stankovic, and D. Zorica. *Fractional Calculus with Applications in Mechanics: Vibrations and Diffusion Processes*. John Wiley & Sons, Hoboken, NJ, 2014.
- [4] L. Banjai, J. M. Melenk, R. H. Nochetto, E. Otárola, A. J. Salgado and Ch. Schwab. *Tensor FEM for Spectral Fractional Diffusion*. Found. Comput. Math., (2018). <https://doi.org/10.1007/s10208-018-9402-3>.
- [5] P. W. Bates. *On some nonlocal evolution equations arising in materials science*. Nonlinear dynamics and evolution equations, vol. 48 of Fields Inst. Commun., pp. 1352. Amer. Math. Soc., Providence, RI, 2006.
- [6] R. E. Bellman. *Dynamic programming*. Princeton University Press, 1957.
- [7] P. Ben-Abdallah et al.. *Heat Superdiffusion in Plasmonic Nanostructure Networks*. Physical review letters, 111(17):174301, 2013.
- [8] A. Borzi and V. Schulz. *Multigrid methods for PDE optimization*. SIAM Review 51(2), 2009, 361-395.
- [9] A. Borzi and V. Schulz. *Computational optimization of systems governed by partial differential equations*. Soc. for Ind. and Appl. Math., Philadelphia, 2012.
- [10] H. J. Bungartz and M. Griebel. *Sparse grids*. Acta numerica 13, 147-269, 2004.
- [11] A. Cichocki and Sh. Amari. *Adaptive Blind Signal and Image Processing: Learning Algorithms and Applications*. Wiley, 2002.
- [12] L. De Lathauwer, B. De Moor, J. Vandewalle. *A multilinear singular value decomposition*. SIAM J. Matrix Anal. Appl., 21 (2000) 1253-1278.
- [13] J. C. De Los Reyes. *Numerical PDE-Constrained Optimization*. SpringerBriefs in Optimization, Springer, Berlin, 2015
- [14] S. Dolgov and I. V. Oseledets. *Solution of linear systems and matrix inversion in the TT-format*. SIAM J. Sci. Comput. 34 (5), 2011, pp. A2718-A2739.
- [15] S. Dolgov, J. Pearson, D. Savostyanov and M. Stoll. *Fast tensor product solvers for optimization problems with fractional differential equations as constraints*. Appl. Math. Comp., 273, 2016, 604-623.
- [16] B. Duan, R. Lazarov and J. Pasciak. *Numerical approximation of fractional powers of elliptic operators*. arXiv:1803.10055v1, 2018.
- [17] G. Duvaut and J. L. Lions. *Inequalities in mechanics and physics*. Grundlehren der Mathematischen Wissenschaften, 219. Springer Verlag, Berlin, 1976.
- [18] I. P. Gavriljuk, W. Hackbusch, and B. N. Khoromskij. *Tensor-product approximation to elliptic and parabolic solution operators in higher dimensions*. Computing **74** (2005), 131-157.
- [19] G. Gilboa and S. Osher. *Nonlocal operators with applications to image processing*. Multiscale Model. Simul., 7(3):10051028, 2008.
- [20] L. Greengard and V. Rokhlin. *A fast algorithm for particle simulations*. J. Comp. Phys. 73 (1987) 325.
- [21] W. Hackbusch. *Tensor spaces and numerical tensor calculus*. Springer, Berlin, 2012.
- [22] W. Hackbusch. *Hierarchical Matrices: Algorithms and Analysis*. Springer, Berlin, 2009.
- [23] W. Hackbusch and B. N. Khoromskij. *Low-rank Kronecker product approximation to multi-dimensional nonlocal operators. Part I. Separable approximation of multi-variate functions*. Computing **76** (2006), 177-202.
- [24] G. Heidel, V. Khoromskaia, B. N. Khoromskij and V. Schulz. *Tensor approach to optimal control problems with fractional d-dimensional elliptic operator in constraints*. arXiv:1809.01971, 2018.
- [25] R. Herzog and K. Kunisch. *Algorithms for PDE constrained optimization*. GAMM, 33 (2010), 163-176.

- [26] N. Hale, N. J. Higham, and L. N. Trefethen. *Computing A^α , $\log(A)$, and related matrix functions by contour integrals*. SIAM J. on Numerical Analysis, 46 (2), 2008, 2505-2523.
- [27] S. Harizanov, R. Lazarov, P. Marinov, S. Margenov and Ya. Vutov. *Optimal solvers for linear systems with fractional powers of sparse spd matrices*. Preprint arXiv:1612.04846v3, 2018.
- [28] N. J. Higham. *Functions of Matrices*. SIAM, Philadelphia, 2008.
- [29] F. L. Hitchcock. *The expression of a tensor or a polyadic as a sum of products*. J. Math. Physics, 6 (1927), 164-189.
- [30] M. Karkulik and J. M. Melenk. *H-matrix approximability of inverses of discretizations of the fractional Laplacian*. Adv Comput Math 45, 28932919 (2019). <https://doi.org/10.1007/s10444-019-09718-5>
- [31] V. Khoromskaia and B. N. Khoromskij. *Tensor Numerical Methods in Quantum Chemistry*. Research monograph, De Gruyter Verlag, Berlin, 2018.
- [32] B. N. Khoromskij. *Structured Rank- (r_1, \dots, r_d) Decomposition of Function-related Tensors in \mathbb{R}^d* . Comp. Meth. Applied Math., 6, (2006), 2, 194-220.
- [33] B. N. Khoromskij. *Tensor-Structured Preconditioners and Approximate Inverse of Elliptic Operators in \mathbb{R}^d* . Constructive Approximation, 30:599-620 (2009).
- [34] B. N. Khoromskij. *Tensor Numerical Methods in Scientific Computing*. Research monograph, De Gruyter Verlag, Berlin, 2018.
- [35] B. N. Khoromskij and V. Khoromskaia. *Low-Rank Tucker-Type Tensor Approximation to Classical Potentials*. Central European J. of Math., 5(3), pp.523-550, 2007.
- [36] B. N. Khoromskij and V. Khoromskaia. *Multigrid Tensor Approximation of Function Related Arrays*. SIAM J. Sci. Comp., 31(4), 3002-3026 (2009).
- [37] T. G. Kolda and B. W. Bader. *Tensor Decompositions and Applications*. SIAM Rev, 51(2009), no. 3, pp.455-500.
- [38] D. Kressner and C Tobler. *Krylov subspace methods for linear systems with tensor product structure*. SIAM J Matr. Anal. Appl., 31 (4), pp. 1688-1714.
- [39] D. Kressner and C. Tobler. *Preconditioned Low-Rank Methods for High-Dimensional Elliptic PDE Eigenvalue Problems*. Computational Methods in Applied Mathematics, 11 (3), pp. 363-381 (2011).
- [40] M. Kwaśnicki. *Ten equivalent definitions of the fractional Laplace operator*. Functional Calculus and Applied Analysis, 20(1):7-51, 2017.
- [41] A. Lischke, G. Pang, M. Gulian, F. Song, Ch. Glusa, X. Zheng, Z. Mao, W. Cei, M. M. Meerschaert, M. Ainsworth, G. E. Karniadakis. *What is the fractional Laplacian?* arXiv:1801.09767v1, 2018.
- [42] F. Stenger. *Numerical methods based on Sinc and analytic functions*. Springer-Verlag, 1993.
- [43] F. Tröltzsch. *Optimal control of partial differential equations: theory, methods and applications*. AMS, Providence, Rhode Island, 2010.
- [44] L. R. Tucker. *Some mathematical notes on three-mode factor analysis*. Psychometrika, 31 (1966) 279-311.
- [45] P. N. Vabishchevich. *Numerically solving an equation for fractional powers of elliptic operators*. J. Comput. Phys., 282, 2015, pp. 289-302.